

INSTITUT NATIONAL DE RECHERCHE EN INFORMATIQUE ET EN AUTOMATIQUE

***A Robust Technique for Matching Two  
Uncalibrated Images Through the Recovery of  
the Unknown Epipolar Geometry***

Zhengyou ZHANG

Rachid DERICHE - Olivier FAUGERAS - Quang-Tuan LUONG

**N° 2273**

May 1994

PROGRAMME 4

Robotique,  
image  
et vision



***rapport  
de recherche***

**1994**



## A Robust Technique for Matching Two Uncalibrated Images Through the Recovery of the Unknown Epipolar Geometry

Zhengyou ZHANG  
Rachid DERICHE - Olivier FAUGERAS - Quang-Tuan LUONG

Programme 4 — Robotique, image et vision  
Projet Robotvis

Rapport de recherche n° 2273 — May 1994 — 38 pages

**Abstract:** This paper proposes a robust approach to image matching by exploiting the only available geometric constraint, namely, the epipolar constraint. The images are uncalibrated, namely the motion between them and the camera parameters are not known. Thus, the images can be taken by different cameras or a single camera at different time instants. If we make an exhaustive search for the epipolar geometry, the complexity is prohibitively high. The idea underlying our approach is to use some classical techniques (correlation and relaxation methods in our particular implementation) to find an initial set of matches, and then use a robust technique—the Least Median of Squares (LMedS)—to discard false matches in this set. The epipolar geometry can then be accurately estimated using a well adapted criterion. More matches are eventually found, as in stereo matching, by using the recovered epipolar geometry. A large number of experiments have been carried out, and very good results have been obtained.

Regarding the relaxation technique, we define a new measure of matching support, which allows a higher tolerance to deformation with respect to rigid transformations in the image plane and a smaller contribution for distant matches than for nearby ones. A new strategy for updating matches is developed, which only selects those matches having both high matching support and low matching ambiguity. The update strategy is different from the classical “winner-take-all”, which is easily stuck at a local minimum, and also from “loser-take-nothing”, which is usually very slow. The proposed algorithm has been widely tested and works remarkably well in a scene with many repetitive patterns.

**Key-words:** Robust Matching, Epipolar Geometry, Fundamental Matrix, Least Median Squares (LMedS), Relaxation, Correlation.

*(Résumé : tsvp)*

## Mise en correspondance robuste d'images non calibrées par recouvrement de la géométrie épipolaire

**Résumé :** Dans cet article, nous proposons une approche robuste au problème de la mise en correspondance de primitives dans le cas d'images non calibrées i.e on ne dispose ni du mouvement entre les caméras ni des paramètres intrinsèques associés à chacune des caméras. Les images peuvent ainsi être considérées comme prises par une même caméra à différents instants ou par un système stéréoscopique de 2 caméras. Dû à la complexité de la tâche, une recherche exhaustive de la géométrie épipolaire ne peut évidemment être entreprise. L'idée principale de l'approche que nous développons est d'utiliser, dans une première phase, des méthodes classiques de type corrélation et relaxation afin de trouver un premier ensemble d'appariements entre points à forte courbure des 2 images. Une seconde phase fait alors appel à des méthodes robustes de type - Moindres médianes des erreurs au carré ( Least Median of Squares ou LMedS) - afin d'éliminer les éventuels faux appariements. La géométrie épipolaire est alors estimée à l'aide de cet ensemble d'appariements et de l'utilisation de critères de minimisation adéquats et bien adaptés au problème de sa détermination. Une ultime phase de recherche des appariements respectant la contrainte de la ligne épipolaire peut alors être effectuée afin d'améliorer encore les résultats. Un grand nombre d'expériences ont été menées et d'excellents résultats ont été obtenus.

Concernant la technique de relaxation utilisée, nous définissons une nouvelle mesure d'appariement qui associe une grande tolérance aux déformations rigides dans le plan image, et qui associe une faible (resp. grande) contribution aux appariements lointains (resp. proches). Une nouvelle stratégie pour la mise à jour des appariements est développée. Elle permet de ne sélectionner que les appariements qui ont un large support de correspondance et un faible score d'ambiguïté. Cette mise à jour est différente de l'approche classique dite "le vainqueur prend tout" (winner-take-all) sujette au problème des minima locaux, et aussi différente de l'approche "le perdant ne gagne rien" (looser take nothing) qui est très lente. L'algorithme proposé a été largement testé et fonctionne remarquablement bien sur des scènes à motifs périodiques.

**Mots-clé :** Mise en correspondance robuste, Géométrie épipolaire, Matrice fondamentale, Moindres médianes (LMedS), Relaxation, Corrélation.

---

## Contents

<b>1</b>	<b>Introduction</b>	<b>3</b>
<b>2</b>	<b>Notation</b>	<b>5</b>
<b>3</b>	<b>Epipolar Geometry</b>	<b>6</b>
<b>4</b>	<b>Finding Candidate Matches by Correlation</b>	<b>8</b>
4.1	Extracting Points of Interest . . . . .	8
4.2	Matching Through Correlation . . . . .	9
<b>5</b>	<b>Disambiguating Matches Through Relaxation</b>	<b>10</b>
5.1	Measure of the Support for a Candidate Match . . . . .	10
5.2	Relaxation Process . . . . .	12
<b>6</b>	<b>Robust Estimation of the Epipolar Geometry</b>	<b>14</b>
6.1	The Linear Criterion . . . . .	14
6.2	Minimizing the Distances to Epipolar Lines . . . . .	15
6.3	Taking into Account Possible Outliers in the Initial Correspondences . . . . .	16
<b>7</b>	<b>Stereo Matching</b>	<b>19</b>
<b>8</b>	<b>Experimental Results</b>	<b>20</b>
<b>9</b>	<b>Conclusion</b>	<b>33</b>

## List of Figures

1	The epipolar geometry . . . . .	6
2	Correlation . . . . .	9
3	Illustration of the non-symmetric problem of the matching support measure .	12
4	Illustration of a bucketing technique . . . . .	18
5	Interval and bucket mapping . . . . .	19
6	Scene <b>bust</b> : Matching result with the correlation technique . . . . .	22
7	Scene <b>bust</b> : Matching result with the relaxation technique and the epipolar geometry recovered using all matched points . . . . .	22
8	Scene <b>bust</b> : The epipolar geometry recovered after discarding outliers and the matched points found using the epipolar constraint . . . . .	23
9	Scene <b>road</b> : Matching result with the correlation technique . . . . .	24
10	Scene <b>road</b> : Matching result with the relaxation technique and the epipolar geometry recovered using all matched points . . . . .	24
11	Scene <b>road</b> : The epipolar geometry recovered after discarding outliers and the matched points found using the epipolar constraint . . . . .	25
12	Scene <b>valley</b> : Matching result with the correlation technique . . . . .	25
13	Scene <b>valley</b> : Matching result with the relaxation technique and the epipolar geometry recovered using all matched points . . . . .	26
14	Scene <b>valley</b> : The epipolar geometry recovered after discarding outliers and the matched points found using the epipolar constraint . . . . .	26
15	Scene <b>rotation</b> : Matching result with the correlation technique . . . . .	27
16	Scene <b>rotation</b> : Matching result with the relaxation technique and the epipolar geometry recovered using all matched points . . . . .	27
17	Scene <b>rotation</b> : The epipolar geometry recovered after discarding outliers and the matched points found using the epipolar constraint . . . . .	28
18	Scene <b>trunk</b> : Matching result with the correlation technique . . . . .	29
19	Scene <b>trunk</b> : Matching result with the relaxation technique and the epipolar geometry recovered using all matched points . . . . .	29
20	Scene <b>trunk</b> : The epipolar geometry recovered after discarding outliers and the matched points found using the epipolar constraint . . . . .	30
21	Scene <b>tracing</b> : Matching result with the correlation technique . . . . .	30
22	Scene <b>tracing</b> : Matching result with the relaxation technique and the epipolar geometry recovered using all matched points . . . . .	31
23	Scene <b>tracing</b> : The epipolar geometry recovered after discarding outliers and the matched points found using the epipolar constraint . . . . .	32

## 1 Introduction

Matching different images of a single scene remains one of the bottlenecks in computer vision. A large amount of work has been carried out during the last 15 years, but the results are, however, not satisfactory. The only geometric constraint we know between two images of a single scene is the *epipolar constraint*. However, when the motion between the two images is not known, the epipolar geometry is also unknown. The methods reported in the literature all exploit some heuristics in one form or another, for example, intensity similarity, which are not applicable to most cases. The difficulty is partly bypassed by taking long sequences of images over short time interval [9, 58]. Indeed, as the time interval is small and object velocity is constrained by physical laws, the interframe displacements of objects are bounded, i.e., the correspondence of a token at the subsequent instant must be in the neighborhood of the first. However, in many cases, such as a pair of uncalibrated stereo images, this technique does not apply. Developing a robust image matching technique is thus very important.

Over the years numerous algorithms for image matching have been proposed. They can roughly be classified into two categories:

1. **Template matching.** In this category, the algorithms attempt to correlate the grey levels of image patches in the views being considered, assuming that they present some similarity [4, 15, 16, 7, 14]. The underlying assumption appears to be a valid one for relatively textured areas and for image pairs with small difference; however it may be wrong at occlusion boundaries and within featureless regions.
2. **Feature matching.** In this category, the algorithms first extract salient primitives from the images, such as edge segments or contours, and match them in two or more views. An image can then be described by a graph with primitives defining the nodes and geometric relations defining the links. The registration of two maps becomes the mapping of the two graphs: *subgraph isomorphism*. Common techniques are tree searching, relaxation, maximal clique detection, etc. Some heuristics such as assuming affine transformation between the two images are usually introduced to reduce the complexity. These methods are fast because only a small subset of the image pixels are used, but may fail if the chosen primitives cannot be reliably detected in the images. The following list of references is by no means exhaustive: [54, 50, 5, 6, 45, 35, 22, 55]

The approach we propose in this paper aims at exploiting the only geometric constraint, i.e., the epipolar constraint, to establish robustly correspondences between two perspective images of a single scene. We first extract high curvature points and then match them using a classical correlation technique followed by a new fuzzy relaxation procedure. More precisely, our algorithm consists of three steps:

- Establish initial correspondences using some classical techniques,
- Estimate robustly the epipolar geometry,
- Establish correspondences using estimated epipolar geometry as in stereo matching.

The basic idea is first to estimate robustly the epipolar geometry, and then reduce the general image matching problem to stereo matching. In the subsequent sections, we will first

review the epipolar geometry, and then describe in detail the three steps of the proposed approach. A preliminary version of this paper appeared in the proceedings of the third European Conference on Computer Vision [12].

A similar idea has been independently exploited by Xu et al. [57, 40], who also searched for image correspondences through the recovery of the epipolar geometry. There are however two main differences:

- The weak perspective camera model is used in their work, and a full perspective model is used in ours. The choice of the most appropriate criterion for the recovery of the epipolar geometry is not addressed in their work.
- The search for the epipolar geometry is carried out with an exhaustive strategy in their work. The complexity is prohibitively high even for a weak perspective model ( $O(m^4n^4)$ , where  $m$  and  $n$  are the number of points in the first and second image, respectively). The complexity is reduced by checking only a few closest points. In our work, some classical techniques are applied to find an initial set of correspondences.

We could apply the same strategy as that of Xu et al. [57, 40]. In fact, it has been applied to solve the correspondence problem between two sets of 3D line segments [59]. When applying it to the problem addressed in this paper, we need 8 point correspondences in order to estimate the epipolar geometry. The complexity is then  $O(m^8n^8)$ . Suppose both  $m$  and  $n$  are 100, the complexity is in the order of  $10^{32}$ ! Xu et al. [57, 40] deal with also the motion segmentation problem using epipolar constraint, which is not addressed in this paper.

Recently, computer vision researchers have paid much attention to the robustness of vision algorithms because the data are unavoidably error prone [17, 60]. Many the so-called *robust regression* methods have been proposed that are not so easily affected by outliers [25, 48]. The reader is referred to [48, Chap. 1] for a review of different robust methods. The two most popular robust methods are the *M-estimators* and the *least-median-of-squares* (LMedS) method (see Sect. 6.3). Kumar and Hanson [26] compared different robust methods for pose refinement from 3D-2D line correspondences, while Meer et al. [38], for image smoothing. Haralick et al. [18] applied M-estimators to solve the pose problem from point correspondences. Thompson et al. [51] applied the LMedS estimator to detect moving objects using point correspondences between orthographic views. Other recent works on the application of robust techniques to motion segmentation include [52, 42, 3].

Regarding the robust recovery of the epipolar geometry, our work is closely related to that of Olsen [43] and that of Shapiro and Brady [49]. Olsen uses a linear method to estimate the epipolar geometry, which has already been shown in one of our previous work [32] to be insufficiently accurate. He further assumes that knowledge of the epipolar geometry, as in many practical cases, is available. In particular, he assumes the epipolar lines are almost aligned horizontally. This knowledge is then used to find matches between the stereo image pair, and a robust method (the M-estimator, see Sect. 6.3) is used to detect false matches and to obtain a better estimate of the epipolar geometry. Shapiro and Brady also use a linear method. The camera model is however a simplified one, namely an affine camera. Correspondences are established by tracking corner features over time. False matches are

rejected through a *regression diagnostic*, which computes an initial estimate of the epipolar geometry over all matches, and sees how the estimate changes if a match is deleted. The match whose removal maximally reduces the residual is identified to be an *outlier* and is rejected. The procedure is then repeated with the reduced set of matches until all outliers have been removed. These two approaches (M-estimators and Regression diagnostics) work well when the percentage of outliers is small and more importantly when their derivations from the valid matches are not too large, as in the above two works. In the case described in this paper, two images can be quite different. There may be a large percentage of false matches (usually around 20%, sometimes 40%) using heuristic matching techniques such as correlation, and a false match may be completely different from the valid matches. The robust technique described in this paper deals with these issues and can theoretically detect outliers when they make up as much as 50% of whole data.

## 2 Notation

A camera is described by the widely used pinhole model. The coordinates of a 3-D point  $M = [x, y, z]^T$  in a world coordinate system and its retinal image coordinates  $\mathbf{m} = [u, v]^T$  are related by

$$s \begin{bmatrix} u \\ v \\ 1 \end{bmatrix} = \mathbb{P} \begin{bmatrix} x \\ y \\ z \\ 1 \end{bmatrix},$$

where  $s$  is an arbitrary scale, and  $\mathbb{P}$  is a  $3 \times 4$  matrix, called the perspective projection matrix. Denoting the homogeneous coordinates of a vector  $\mathbf{x} = [x, y, \dots]^T$  by  $\tilde{\mathbf{x}}$ , i.e.,  $\tilde{\mathbf{x}} = [x, y, \dots, 1]^T$ , we have  $s\tilde{\mathbf{m}} = \mathbb{P}\tilde{M}$ .

The matrix  $\mathbb{P}$  can be decomposed as

$$\mathbb{P} = \mathbf{A} [\mathbf{R} \ \mathbf{t}],$$

where  $\mathbf{A}$  is a  $3 \times 3$  matrix, mapping the normalized image coordinates to the retinal image coordinates, and  $(\mathbf{R}, \mathbf{t})$  is the 3D displacement (rotation and translation) from the world coordinate system to the camera coordinate system. The most general matrix  $\mathbf{A}$  can be written as

$$\mathbf{A} = \begin{bmatrix} -fk_u & fk_u \cot \theta & u_0 \\ 0 & -\frac{fk_v}{\sin \theta} & v_0 \\ 0 & 0 & 1 \end{bmatrix}, \quad (1)$$

where

- $f$  is the focal length of the camera,
- $k_u$  and  $k_v$  are the horizontal and vertical scale factors, whose inverses characterize the size of the pixel in the world coordinate unit,

- $u_0$  and  $v_0$  are the coordinates of the principal point of the camera, i.e., the intersection between the optical axis and the image plane, and
- $\theta$  is the angle between the retinal axes. This parameter is introduced to account for the fact that the pixel grid may not be exactly orthogonal. In practice, however, it is very close to  $\pi/2$ .

As is clear, we cannot separate  $f$  from  $k_u$  and  $k_v$ . We thus have five intrinsic parameters for each camera:  $\alpha_u = -fk_u$ ,  $\alpha_v = -fk_v$ ,  $u_0$ ,  $v_0$  and  $\theta$ .

The first and second images are respectively denoted by  $I_1$  and  $I_2$ . A point  $\mathbf{m}$  in the image plane  $I_i$  is noted as  $\mathbf{m}_i$ . The second subscript, if any, will indicate the index of the point in consideration.

### 3 Epipolar Geometry

Considering the case of two cameras as shown in Fig.1. Let  $C_1$  and  $C_2$  be the optical centers of the first and second cameras, respectively. Given a point  $\mathbf{m}_1$  in the first image, its corresponding point in the second image is constrained to lie on a line called the *epipolar line* of  $\mathbf{m}_1$ , denoted by  $\mathbf{l}_{\mathbf{m}_1}$ . The line  $\mathbf{l}_{\mathbf{m}_1}$  is the intersection of the plane  $\Pi$ , defined by  $\mathbf{m}_1$ ,  $C_1$  and  $C_2$  (known as the *epipolar plane*), with the second image plane  $I_2$ . This is because image point  $\mathbf{m}_1$  may correspond to an arbitrary point on the semi-line  $C_1M$  ( $M$  may be at infinity) and that the projection of  $C_1M$  on  $I_2$  is the line  $\mathbf{l}_{\mathbf{m}_1}$ . Furthermore, one observes that all epipolar lines of the points in the first image pass through a common point  $\mathbf{e}_2$ , which is called the *epipole*.  $\mathbf{e}_2$  is the intersection of the line  $C_1C_2$  with the image plane  $I_2$ . This can be easily understood as follows. For each point  $\mathbf{m}_{1k}$  in the first image  $I_1$ , its epipolar line  $\mathbf{l}_{\mathbf{m}_{1k}}$  in  $I_2$  is the intersection of the plane  $\Pi^k$ , defined by  $\mathbf{m}_{1k}$ ,  $C_1$  and  $C_2$ , with image plane  $I_2$ . All epipolar planes  $\Pi^k$  thus form a pencil of planes containing the line  $C_1C_2$ . They must intersect  $I_2$  at a common point, which is  $\mathbf{e}_2$ . Finally, one can easily see the symmetry of the epipolar geometry. The corresponding point in the first image of each point  $\mathbf{m}_{2k}$  lying on  $\mathbf{l}_{\mathbf{m}_{1k}}$  must lie on the epipolar line  $\mathbf{l}_{\mathbf{m}_{2k}}$ , which is the intersection of the same plane  $\Pi^k$  with the first image plane  $I_1$ . All epipolar lines form a pencil containing the epipole  $\mathbf{e}_1$ , which is the intersection of the line  $C_1C_2$  with the image plane  $I_1$ . The symmetry leads to the following observation. If  $\mathbf{m}_1$  (a point in  $I_1$ ) and  $\mathbf{m}_2$  (a point in  $I_2$ ) correspond to a single physical point  $M$  in space, then  $\mathbf{m}_1$ ,  $\mathbf{m}_2$ ,  $C_1$  and  $C_2$  must lie in a single plane. This is the well-known *co-planarity constraint* or *epipolar equation* in solving motion and structure from motion problems when the intrinsic parameters of the cameras are known [29].

Let the displacement from the first camera to the second be  $(\mathbf{R}, \mathbf{t})$ . Let  $\mathbf{m}_1$  and  $\mathbf{m}_2$  be the images of a 3-D point  $M$  on the cameras. Without loss of generality, we assume that  $M$  is expressed in the coordinate frame of the first camera. Under the pinhole model, we have

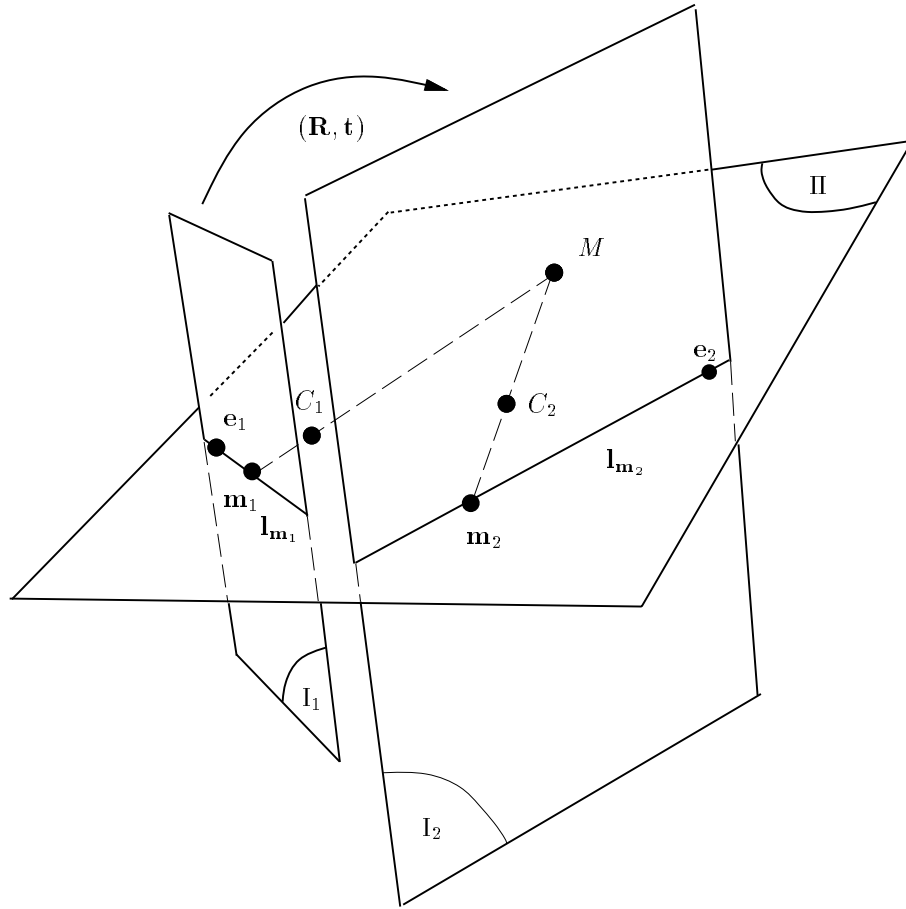


Fig. 1. The epipolar geometry

the following two equations:

$$\begin{aligned} s_1 \tilde{\mathbf{m}}_1 &= \mathbf{A}_1 [\mathbf{I} \ \mathbf{0}] \begin{bmatrix} M \\ 1 \end{bmatrix} \\ s_2 \tilde{\mathbf{m}}_2 &= \mathbf{A}_2 [\mathbf{R} \ \mathbf{t}] \begin{bmatrix} M \\ 1 \end{bmatrix}, \end{aligned}$$

where  $\mathbf{A}_1$  and  $\mathbf{A}_2$  are the intrinsic matrices of the first and second cameras, respectively. Eliminating  $M$ ,  $s_1$  and  $s_2$  from the above equations, we obtain the following fundamental equation

$$\tilde{\mathbf{m}}_2^T \mathbf{A}_2^{-T} \mathbf{T} \mathbf{R} \mathbf{A}_1^{-1} \tilde{\mathbf{m}}_1 = 0, \quad (2)$$

where  $\mathbf{T}$  is an antisymmetric matrix defined by  $\mathbf{t}$  such that  $\mathbf{T}\mathbf{x} = \mathbf{t} \wedge \mathbf{x}$  for all 3-D vector  $\mathbf{x}$  ( $\wedge$  denotes the cross product).

Equation (2) is a fundamental constraint underlying any two images if they are perspective projections of one and the same scene. Let  $\mathbf{F} = \mathbf{A}_2^{-T} \mathbf{T} \mathbf{R} \mathbf{A}_1^{-1}$ ,  $\mathbf{F}$  is known as the fundamental matrix of the two images [31]. Without considering 3-D metric entities, we can think of the fundamental matrix as providing the two epipoles (i.e., the vertexes of the two pencils of epipolar lines) and the 3 parameters of the homography between these two pencils. This is the only geometric information available from two uncalibrated images [36, 31]. This implies that the fundamental matrix has only seven degrees of freedom. Indeed, it is only defined up to a scale factor and its determinant is zero. Geometrically,  $\mathbf{F}\mathbf{m}_1$  defines the epipolar line of point  $\mathbf{m}_1$  in the second image. Equation 2 says no more than that the correspondence in the right image of point  $\mathbf{m}_1$  lies on the corresponding epipolar line. Transposing equation 2 yields the symmetric relation from the second image to the first image.

It can be shown that the fundamental matrix  $\mathbf{F}$  is related to the essential matrix  $\mathbf{E} = \mathbf{t} \times \mathbf{R}$  [29, 23] by

$$\mathbf{F} = \mathbf{A}_2^{-T} \mathbf{E} \mathbf{A}_1^{-1} .$$

It is thus clear that if the cameras are calibrated, the problem becomes the one of *motion and structure from motion* [29, 53, 39, 13, 1, 56, 24].

## 4 Finding Candidate Matches by Correlation

Before recovering the epipolar geometry, we must establish a few correspondences between images. To this end, a corner detector is first applied to each image to extract high curvature points. A classical correlation technique is then used to establish matching candidates between the two images.

### 4.1 Extracting Points of Interest

First, feature points corresponding to high curvature points are extracted from each image. A great deal of effort has been spent by the computer vision community on this problem, and several approaches have been reported in the literature in the last few years. They can be broadly divided into two groups: The first group consists in first extracting edges as a chain code, and then searching for points having maxima curvature [10, 2, 37] or performing a polygonal approximation on the chains and then searching for the line segment intersections [21]. The second group works directly on a grey-level image. The large number of techniques that have been proposed within this group are generally based on the measurement of the gradients and of the curvatures of the surface (see [11] for a review).

In our application, we use the corner detector [19], which is a slightly modified version of the Plessey corner detector [20, 41]. It is based on the following operator:

$$R(x, y) = \det[\hat{C}] - k \text{trace}^2[\hat{C}] , \quad (3)$$

where  $\hat{C}$  is the following matrix:

$$\hat{C} = \begin{bmatrix} \widehat{I_x^2} & \widehat{I_x I_y} \\ \widehat{I_x I_y} & \widehat{I_y^2} \end{bmatrix}, \quad (4)$$

where  $\hat{I}$  denotes the smoothing operation on the grey level image  $I(x, y)$ .  $I_x$  and  $I_y$  indicate the  $x$  and  $y$  directional derivatives respectively.

We use a value of  $k$  equal to 0.04 to provide discrimination against high contrast pixel step edges. After that, the operator output is thresholded for the corner detection. It should be pointed out that this method allows us to recover a corner position up to pixel precision. In order to recover the corner position up to sub-pixel position, one uses the model based approach we have already developed and presented in [8], where corners are extracted directly from the image by searching the parameters of the parametric model that best approximate the observed grey level image intensities around the corner position detected. One can notice that such an approach is well adapted for scenes containing polyhedral objects, but not for most outdoor scenes.

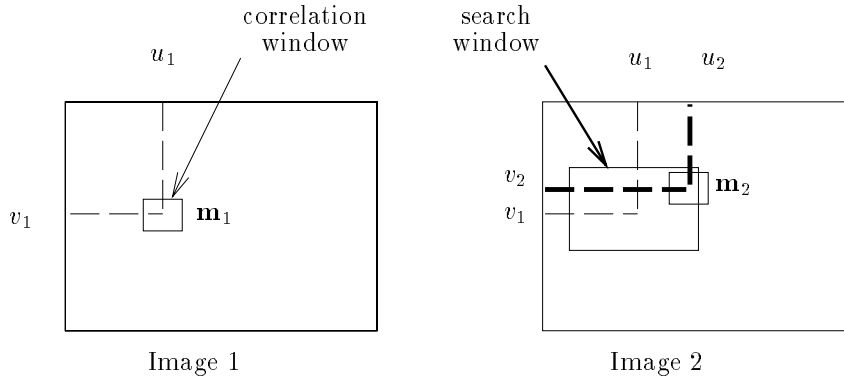


Fig. 2. Correlation

## 4.2 Matching Through Correlation

Given a high curvature point  $\mathbf{m}_1$  in image 1, we use a correlation window of size  $(2n + 1) \times (2m + 1)$  centered at this point. We then select a rectangular search area of size  $(2d_u + 1) \times (2d_v + 1)$  around this point in the second image, and perform a correlation operation on a given window between point  $\mathbf{m}_1$  in the first image and all high curvature points  $\mathbf{m}_2$  lying within the search area in the second image. The search window reflects some *a priori* knowledge about the disparities between the matched points. This is equivalent to reducing the search area for a corresponding point from the whole image to a given window. The

correlation score is defined as

$$Score(\mathbf{m}_1, \mathbf{m}_2) = \frac{\sum_{i=-n}^n \sum_{j=-m}^m [I_1(u_1 + i, v_1 + j) - \overline{I_1(u_1, v_1)}] \times [I_2(u_2 + i, v_2 + j) - \overline{I_2(u_2, v_2)}]}{(2n + 1)(2m + 1)\sqrt{\sigma^2(I_1) \times \sigma^2(I_2)}}, \quad (5)$$

where  $\overline{I_k(u, v)} = \sum_{i=-n}^n \sum_{j=-m}^m I_k(u + i, v + j) / [(2n + 1)(2m + 1)]$  is the average at point  $(u, v)$  of  $I_k$  ( $k = 1, 2$ ), and  $\sigma(I_k)$  is the standard deviation of the image  $I_k$  in the neighborhood  $(2n + 1) \times (2m + 1)$  of  $(u, v)$ , which is given by:

$$\sigma(I_k) = \sqrt{\frac{\sum_{i=-n}^n \sum_{j=-m}^m I_k^2(u, v)}{(2n + 1)(2m + 1)} - \overline{I_k(u, v)}}. \quad (6)$$

The score ranges from  $-1$ , for two correlation windows which are not similar at all, to  $1$ , for two correlation windows which are identical.

A constraint on the correlation score is then applied in order to select the most consistent matches: For a given couple of points to be considered as a candidate match, the correlation score must be higher than a given threshold. If the above constraint is fulfilled, we say that the pair of points considered is self consistent and forms a *candidate match*. For each point in the first image, we thus have a set of candidate matches from the second image (the set is possibly nil); and in the same time we have also a set of candidate matches from the first image for each point in the second image.

In our implementation,  $n = m = 7$  for the correlation window, and a threshold of  $0.8$  on the correlation score is used. For the search window,  $d_u$  and  $d_v$  are set to a quarter of the image width and height, respectively. It is thus very large (half of the whole image).

## 5 Disambiguating Matches Through Relaxation

Using the correlation technique described above, a point in the first image may be paired to several points in the second image (which we call *candidate matches*), and vice versa. Several techniques exist for resolving the matching ambiguities. The technique we use falls into the class of techniques known as *relaxation techniques*. The idea is to allow the candidate matches to reorganize themselves by propagating some constraints, such as continuity and uniqueness, through the neighborhood.

### 5.1 Measure of the Support for a Candidate Match

Consider a candidate match  $(\mathbf{m}_{1i}, \mathbf{m}_{2j})$  where  $\mathbf{m}_{1i}$  is a point in the first image and  $\mathbf{m}_{2j}$  is a point in the second image. Let  $\mathcal{N}(\mathbf{m}_{1i})$  and  $\mathcal{N}(\mathbf{m}_{2j})$  be, respectively, the neighbors of  $\mathbf{m}_{1i}$  and  $\mathbf{m}_{2j}$  within a disc of radius  $R$ . If  $(\mathbf{m}_{1i}, \mathbf{m}_{2j})$  is a good match, we will expect to see many matches  $(\mathbf{n}_{1k}, \mathbf{n}_{2l})$ , where  $\mathbf{n}_{1k} \in \mathcal{N}(\mathbf{m}_{1i})$  and  $\mathbf{n}_{2l} \in \mathcal{N}(\mathbf{m}_{2j})$ , such that the position of  $\mathbf{n}_{1k}$

relative to  $\mathbf{m}_{1i}$  is similar to that of  $\mathbf{n}_{2l}$  relative to  $\mathbf{m}_{2j}$ . On the other hand, if  $(\mathbf{m}_{1i}, \mathbf{m}_{2j})$  is a bad match, we will expect to see only few matches, or even not any at all, in their neighborhood.

More formally, we define a measure of support for a match, which we call the *strength of the match* (SM for abbreviation), as

$$S_M(\mathbf{m}_{1i}, \mathbf{m}_{2j}) = c_{ij} \sum_{\mathbf{n}_{1k} \in \mathcal{N}(\mathbf{m}_{1i})} \left[ \max_{\mathbf{n}_{2l} \in \mathcal{N}(\mathbf{m}_{2j})} \frac{c_{kl} \delta(\mathbf{m}_{1i}, \mathbf{m}_{2j}; \mathbf{n}_{1k}, \mathbf{n}_{2l})}{1 + \text{dist}(\mathbf{m}_{1i}, \mathbf{m}_{2j}; \mathbf{n}_{1k}, \mathbf{n}_{2l})} \right],$$

where  $c_{ij}$  and  $c_{kl}$  are the goodness of the candidate matches  $(\mathbf{m}_{1i}, \mathbf{m}_{2j})$  and  $(\mathbf{n}_{1k}, \mathbf{n}_{2l})$ , which can be the correlation scores given in the last section,  $\text{dist}(\mathbf{m}_{1i}, \mathbf{m}_{2j}; \mathbf{n}_{1k}, \mathbf{n}_{2l})$  is the average distance of the two pairings, i.e.,

$$\text{dist}(\mathbf{m}_{1i}, \mathbf{m}_{2j}; \mathbf{n}_{1k}, \mathbf{n}_{2l}) = [d(\mathbf{m}_{1i}, \mathbf{n}_{1k}) + d(\mathbf{m}_{2j}, \mathbf{n}_{2l})]/2$$

with  $d(\mathbf{m}, \mathbf{n}) = \|\mathbf{m} - \mathbf{n}\|$ , the Euclidean distance between  $\mathbf{m}$  and  $\mathbf{n}$ , and

$$\delta(\mathbf{m}_{1i}, \mathbf{m}_{2j}; \mathbf{n}_{1k}, \mathbf{n}_{2l}) = \begin{cases} e^{-r/\varepsilon_r} & \text{if } (\mathbf{n}_{1k}, \mathbf{n}_{2l}) \text{ is a candidate match and } r < \varepsilon_r \\ 0 & \text{otherwise} \end{cases}$$

where  $r$  is the relative distance difference given by

$$r = \frac{|d(\mathbf{m}_{1i}, \mathbf{n}_{1k}) - d(\mathbf{m}_{2j}, \mathbf{n}_{2l})|}{\text{dist}(\mathbf{m}_{1i}, \mathbf{m}_{2j}; \mathbf{n}_{1k}, \mathbf{n}_{2l})}$$

and  $\varepsilon_r$  is a threshold on the relative distance difference. The above definition of the strength of a match is similar in the form to that used in the PMF stereo algorithm [44].

Several remarks can be made regarding our measure of matching support.

- Firstly, the strength of a match actually counts the number of candidate matches found in the neighborhoods, but only those whose positions relative to the considered match are similar are counted.
- Secondly, the test of similarity in relative positions is based on the relative distance (the value of  $r$ ). Indeed, the similarity in relative positions is justified by the hypothesis that an affine transformation can approximate the change between the neighborhoods of the candidate match being considered. This assumption is reasonable only for a small neighborhood. Thus we should allow larger tolerance in distance differences for distant points, and this is exactly what our criterion does.
- Thirdly, the contribution of a candidate match  $(\mathbf{n}_{1k}, \mathbf{n}_{2l})$  to the strength of the match  $(\mathbf{m}_{1i}, \mathbf{m}_{2j})$  is the exponential of the negative relative error  $r$ , which is strictly monotonically decreasing function of  $r$ . When  $r$  is very big, then  $\exp(-r/\varepsilon_r) \rightarrow 0$ , and the candidate match can be ignored. When  $r \rightarrow 0$ , i.e., the difference is very small, then  $\exp(-r/\varepsilon_r) \rightarrow 1$ , and the candidate will largely contribute to the match  $(\mathbf{m}_{1i}, \mathbf{m}_{2j})$ .

- Fourthly, if a point in the left image has several candidate matches in the right image, only the one which has smallest distance difference is accounted for, which is done by the “max” operator.
- Lastly, the contribution of each candidate match in the neighborhood is weighted by its distance to the match. The addition of ‘1’ is only to prevent the over weight for very close points. In other words, a close candidate match gives more support to the match being considered than a distant one. This is also connected to the fact that an affine approximation is only reasonable for a small neighborhood.

The measure of matching support defined above, however, is not symmetric. That is, the strength of a match is possibly not the same if we reverse the role of the two images, i.e., possibly we have  $S_M(\mathbf{m}_{1i}, \mathbf{m}_{2j}) \neq S_M(\mathbf{m}_{2j}, \mathbf{m}_{1i})$ . This occurs when several points  $\mathbf{n}_{1k} \in \mathcal{N}(\mathbf{m}_{1i})$  are candidate matches of a single point  $\mathbf{n}_{2l} \in \mathcal{N}(\mathbf{m}_{2j})$ , as illustrated in Fig.3 where  $\mathbf{n}_{11}$  and  $\mathbf{n}_{12}$  share the same point  $\mathbf{n}_{21}$  as their candidate match. In our implementation,

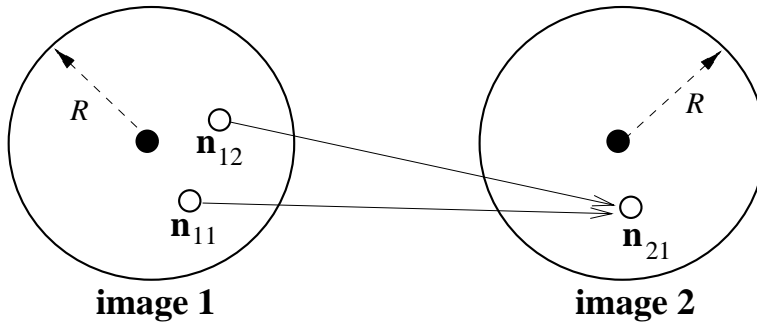


Fig. 3. Illustration of the non-symmetric problem of the matching support measure

we have made the following modification in order to achieve the symmetry. Before computing the summation, if several points  $\mathbf{n}_{1k} \in \mathcal{N}(\mathbf{m}_{1i})$  score the maximal value with the same point  $\mathbf{n}_{2l} \in \mathcal{N}(\mathbf{m}_{2j})$ , then only the point which gives the largest value is counted. This assures that the same pairing will be counted if we reverse the role of the two images.

Other heuristics can be integrated into the computation of the strength of a match. For example, if the angle of the rotation in the image plane is assumed to be less than  $\Theta$ , then we can impose the following constraint: the angle between  $\overline{\mathbf{m}_{1i}\mathbf{n}_{1k}}$  and  $\overline{\mathbf{m}_{2j}\mathbf{n}_{2l}}$  must be less than  $\Theta$ . In other words, for a candidate match  $(\mathbf{n}_{1k}, \mathbf{n}_{2l})$  which does not satisfy the above constraint, its  $\delta(\mathbf{m}_{1i}, \mathbf{m}_{2j}; \mathbf{n}_{1k}, \mathbf{n}_{2l})$  takes the value of zero.

In our implementation,  $R =$  one eighth of the image width,  $c_{ij} = 1$ ,  $\varepsilon_r = 0.3$  and  $\Theta = 90^\circ$ .

## 5.2 Relaxation Process

If we define the energy function as the sum of the strengths of all candidate matches, i.e.,

$$\mathcal{J} = \sum_{(\mathbf{m}_{1i}, \mathbf{m}_{2j})} S_M(\mathbf{m}_{1i}, \mathbf{m}_{2j})$$

then the problem of disambiguating matches is equivalent to minimizing the energy function  $\mathcal{J}$ . The relaxation scheme is one approach to it. It is an iterative procedure, and can be formulated as follows:

- iterate** {
- compute the matching strength for each candidate match
  - update the matches by minimizing the total energy
- } until the convergence of the energy**

After the correlation procedure, for each point in the first image, we have a set of candidate matches from the second image (the set is possibly nil); and in the same time we have also a set of candidate matches from the first image for each point in the second image. The last subsection has already explained how to compute the SM for each candidate match. As the definition of SM is now symmetric, we only need to compute SMs for the list of candidate matches in the left image and assign the values to the candidate matches in the right image, thus saving half of the computation.

There are several strategies for updating the matching in order to minimize the total energy. The first is the “*winner-take-all*”, as exploited by Rosenfeld et al. [47], Zucker et al. [61], and Pollard et al. [44]. The method works as follows. At each iteration, any matches which have the highest matching strengths for both of the two image points that formed them are immediately chosen as “correct”. That is, a match  $(\mathbf{m}_{1i}, \mathbf{m}_{2j})$  is selected if its points (either  $\mathbf{m}_{1i}$  or  $\mathbf{m}_{2j}$ ) have no higher matching-strength scores with any other matches they can form. Then, because of the uniqueness constraint, all other matches associated with the two points in each chosen match are eliminated from further consideration. This allows further matches, that were not previously either selected or eliminated, to be selected as correct provided they now have the highest matching strengths for both constituent points. This method proceeds as a steepest-descent approach, and is thus fast. However, it may get stuck easily at a bad local minimum.

The second is the “*looser-take-nothing*” [28]. The method works as follows. For each point in the first image, the candidate which has gained the weakest matching strength is eliminated. The process suppresses at most one candidate at each iteration until one and only one candidate is left for each point, finally achieving an unambiguous set of matches. Since the suppressed matches have gained the weakest support, they are very possibly not among the correct matches. This method thus proceeds as a slowest-descent approach, and is not efficient if a point has many candidate matches. Furthermore, this method is not symmetric for the two images: reversing the role of the two images may give different result.

We have developed a new update strategy, which we would like to call “*some-winners-take-all*”. It differs from “winner-take-all”, which is in fact *all-winners-take-all*, and works as follows. As with “winner-take-all”, we consider all matches which have the highest matching strength for both of the two image points that formed them. We shall call such matches the *potential matches*, and denote them by  $\{\mathcal{P}_i\}$ . For  $\{\mathcal{P}_i\}$ , we construct two tables. The first, denoted by  $\mathcal{T}_{SM}$ , saves the matching strength of each  $\mathcal{P}_i$ , and is then sorted in decreasing order. The second, denoted by  $\mathcal{T}_{UA}$ , saves a value which indicates how unambiguous each  $\mathcal{P}_i$  is. This is defined as

$$U_A = 1 - S_M^{(2)} / S_M^{(1)},$$

where  $S_M^{(1)}$  is the SM of  $\mathcal{P}_i$ , and  $S_M^{(2)}$  is the SM of the second best candidate match. Thus  $U_A$  is ranging from 1 (unambiguous) to 0 (ambiguous). The table  $\mathcal{T}_{UA}$  is also sorted in decreasing order. Finally, those potential matches  $\mathcal{P}_i$  which are among both the first  $q$  percent of matches in  $\mathcal{T}_{SM}$  and the first  $q$  percent of matches in  $\mathcal{T}_{UA}$  are selected as correct matches. Thus, ambiguous potential matches will not be selected even they have high SM, and those having weak SM will not be selected even they are unambiguous. We have therefore prevented the problem of evolve-too-soon-ness with “winner-take-all” while maintaining computational efficiency. If a candidate match does not receive any support ( $S_M = 0$ ), it will be eliminated from further consideration. If  $q = 100$ , i.e., one hundred percent selection case, our method becomes “winner-take-all”. Not that  $q$  must be larger than 50 in order to assure that at least one potential match will be selected at each iteration if there exist several potential matches. If  $q < 50$ , a premature stop may occur. In our implementation,  $q$  is set to 60.

Our algorithm necessarily converges, because if during one iteration there is no match selected, then the total energy will remain the same at the next iteration. The number of selected matches is evidently limited because the number of candidate matches is limited.

## 6 Robust Estimation of the Epipolar Geometry

Using the set of matched points established in the previous step, one may then recover the so-called fundamental matrix. This is one of the most crucial steps. We will consider linear and nonlinear criteria and also exploit a robust technique to detect the outliers in the correspondences.

### 6.1 The Linear Criterion

Equation (2) can be written as a linear and homogeneous equation in the 9 unknown coefficients of matrix  $\mathbf{F}$ :

$$\mathbf{u}^T \mathbf{f} = 0, \tag{7}$$

where

$$\begin{aligned} \mathbf{u} &= [u_1 u_2, v_1 u_2, u_2, u_1 v_2, v_1 v_2, v_2, u_1, v_1, 1]^T \\ \mathbf{f} &= [F_{11}, F_{12}, F_{13}, F_{21}, F_{22}, F_{23}, F_{31}, F_{32}, F_{33}]^T. \end{aligned}$$

Thus we know that if we are given 8 matches we will be able, in general, to determine a unique solution for  $\mathbf{F}$ , defined up to a scale factor. This approach, known as the eight point algorithm, was introduced by Longuet-Higgins [29] for solving the motion and structure from motion problem, and has been extensively studied in the literature [30, 53, 56, 27] for the computation of the *Essential matrix*  $E$  (see Sect.3). It has proven to be very sensitive to noise.

In practice, we are given many more than 8 matches and we use a least-squares method to solve

$$\min_{\mathbf{F}} \sum_i (\tilde{\mathbf{m}}_{2i}^T \mathbf{F} \tilde{\mathbf{m}}_{1i})^2, \quad (8)$$

which can be rewritten as:

$$\min_{\mathbf{f}} \|\mathbf{U}\mathbf{f}\|^2,$$

where

$$\mathbf{U} = \begin{bmatrix} \mathbf{u}_1^T \\ \vdots \\ \mathbf{u}_n^T \end{bmatrix}.$$

Several methods are possible to solve this problem. The first uses a closed-form solution via the linear equations by setting one of the coefficients of  $\mathbf{F}$  to 1. The second solves the classical problem:

$$\min_{\mathbf{f}} \|\mathbf{U}\mathbf{f}\|^2 \quad \text{subject to } \|\mathbf{f}\| = 1. \quad (9)$$

The solution is the eigenvector of  $\mathbf{U}^T \mathbf{U}$  associated with the smallest eigenvalue.

The advantage of the linear criterion is that it leads to a non-iterative computation method, however, we have found that it is quite sensitive to noise, even with a large set of data points. The two main reasons for this are:

- The constraint  $\det(\mathbf{F}) = 0$  is not satisfied, which causes inconsistencies of the epipolar geometry near the epipoles.
- The criterion is not normalized, which causes a bias in the localization of the epipoles.

The reader is referred to [32] for a detailed study of the linear methods.

## 6.2 Minimizing the Distances to Epipolar Lines

As it has been said, one of the drawbacks of the linear criterion method is that we do not take into account the fact that the rank of  $\mathbf{F}$  is only two, and that  $\mathbf{F}$  thus depends on only 7 parameters. This could be taken into account by parameterizing matrix  $\mathbf{F}$  as follows:

$$\mathbf{F} = \begin{pmatrix} b & a & -ay - bx \\ -d & -c & cy + dx \\ dy' - bx' & cy' - ax' & -cyy' - dy'x + ayx' + bxx' \end{pmatrix}, \quad (10)$$

where the parameters  $(x, y)$  and  $(x', y')$  are the affine coordinate of the two epipoles, and the coefficients, of the homography between the two pencils of epipolar lines, which are the coefficients of the sub-matrix  $2 \times 2$  obtained by suppressing the third line and the third column. However, nonlinear minimizations must be performed.

The first idea is to use a nonlinear criterion by minimizing:

$$\sum_i d^2(\tilde{\mathbf{m}}_{2i}, \mathbf{F}\tilde{\mathbf{m}}_{1i}),$$

where  $d(\tilde{\mathbf{m}}_2, \mathbf{F}\tilde{\mathbf{m}}_1)$  is the Euclidean distance of point  $\tilde{\mathbf{m}}_2$  to its epipolar line  $\mathbf{F}\tilde{\mathbf{m}}_1$ . It is given by

$$d(\tilde{\mathbf{m}}_2, \mathbf{F}\tilde{\mathbf{m}}_1) = \frac{|\tilde{\mathbf{m}}_2^T \mathbf{F}\tilde{\mathbf{m}}_1|}{\sqrt{(\mathbf{F}\tilde{\mathbf{m}}_1)_1^2 + (\mathbf{F}\tilde{\mathbf{m}}_1)_2^2}},$$

where  $(\mathbf{F}\tilde{\mathbf{m}}_1)_i$  is the  $i$ -th component of vector  $\mathbf{F}\tilde{\mathbf{m}}_1$ . However, unlike the case of the linear criterion, the two images do not play a symmetric role. To obtain a consistent epipolar geometry, it is necessary and sufficient that by exchanging the two images, the fundamental matrix is changed to its transpose. This yields the following criterion:

$$\sum_i (d^2(\tilde{\mathbf{m}}_{2i}, \mathbf{F}\tilde{\mathbf{m}}_{1i}) + d^2(\tilde{\mathbf{m}}_{1i}, \mathbf{F}^T \tilde{\mathbf{m}}_{2i})),$$

which operates simultaneously in the two images. Using the fact that  $\tilde{\mathbf{m}}_2^T \mathbf{F}\tilde{\mathbf{m}}_1 = \tilde{\mathbf{m}}_1^T \mathbf{F}^T \tilde{\mathbf{m}}_2$ , it can be rewritten as:

$$\sum_i \left( \frac{1}{(\mathbf{F}\tilde{\mathbf{m}}_{1i})_1^2 + (\mathbf{F}\tilde{\mathbf{m}}_{1i})_2^2} + \frac{1}{(\mathbf{F}^T \tilde{\mathbf{m}}_{2i})_1^2 + (\mathbf{F}^T \tilde{\mathbf{m}}_{2i})_2^2} \right) (\tilde{\mathbf{m}}_{2i}^T \mathbf{F}\tilde{\mathbf{m}}_{1i})^2. \quad (11)$$

This criterion is also clearly normalized in the sense that it does not depend on the scale factor used to compute  $\mathbf{F}$ .

### 6.3 Taking into Account Possible Outliers in the Initial Correspondences

In all matches established so far, as described in section 5, we may find two types of *outliers* due to

**bad locations.** In the estimation of the fundamental matrix, the location error of a point of interest is assumed to exhibit Gaussian behavior. This assumption is reasonable since the error in localization for most points of interest is small (within one or two pixels), but a few points are possibly incorrectly localized (more than three pixels). The latter points will severely degrade the accuracy of the estimation.

**false matches.** In the establishment of correspondences, only heuristics have been used. Because the only geometric constraint, i.e., the epipolar constraint in terms of the

*fundamental matrix*, is not yet available, many matches are possibly false. These will completely spoil the estimation process, and the final estimate of the fundamental matrix will be useless.

The outliers will severely affect the precision of the fundamental matrix if we directly apply the methods described above. In the following, we give a brief description of the two most popular robust methods: the *M-estimators* and the *least-median-of-squares* (LMedS) method.

Let  $r_i$  be the *residual* of the  $i$ -th datum, i.e., the difference between the  $i$ -th observation and its fitted value. The standard least-squares method tries to minimize  $\sum_i r_i^2$ , which is unstable if there are outliers present in the data. The M-estimators replace the squared residuals  $r_i^2$  by another functions of the residuals, yielding

$$\min \sum_i \rho(r_i) ,$$

where  $\rho$  is a symmetric, positive-definite function with a unique minimum at zero. For example, Huber [25] employed the squared error for small residuals and the absolute error for large residuals. The M-estimators can be implemented as a weighted least-squares problem. In [43, 31], the following weight was used for the estimation of the epipolar geometry:

$$w_i = \begin{cases} 1 & |r_i| \leq \sigma \\ \sigma/|r_i| & \sigma < |r_i| \leq 3\sigma \\ 0 & 3\sigma < |r_i| , \end{cases}$$

where  $\sigma$  is some estimated standard deviation of errors. This method was robust to outliers due to bad localization. It was, however, not robust to false matches.

The LMedS method estimates the parameters by solving the nonlinear minimization problem:

$$\min \operatorname{med}_i r_i^2 .$$

That is, the estimator must yield the smallest value for the median of squared residuals computed for the entire data set. It turns out that this method is very robust to false matches as well as outliers due to bad localization. Unlike the M-estimators, however, the LMedS problem cannot be reduced to a weighted least-squares problem. It is probably impossible to write down a straightforward formula for the LMedS estimator. It must be solved by a search in the space of possible estimates generated from the data. Since this space is too large, only a randomly chosen subset of data can be analyzed. The algorithm which we have implemented for robustly estimating the fundamental matrix follows that structured in [48, Chap. 5], as outlined below.

Given  $n$  point correspondences:  $\{(\mathbf{m}_{1i}, \mathbf{m}_{2i})\}$ . A Monte Carlo type technique is used to draw  $m$  random subsamples of  $p = 8$  different point correspondences. For each subsample, indexed by  $J$ , we determine the fundamental matrix  $\mathbf{F}_J$ . For each  $\mathbf{F}_J$ , we can determine

the median of the squared residuals, denoted by  $M_J$ , with respect to the whole set of point correspondences, i.e.,

$$M_J = \underset{i=1, \dots, n}{\text{med}} [d^2(\tilde{\mathbf{m}}_{2i}, \mathbf{F}_J \tilde{\mathbf{m}}_{1i}) + d^2(\tilde{\mathbf{m}}_{1i}, \mathbf{F}_J^T \tilde{\mathbf{m}}_{2i})] .$$

We retain the estimate  $\mathbf{F}_J$  for which  $M_J$  is minimal among all  $m$   $M_J$ 's. The question now is: *How do we determine  $m$ ?* A subsample is “good” if it consists of  $p$  good correspondences. Assuming that the whole set of correspondences may contain up to a fraction  $\varepsilon$  of outliers, the probability that at least one of the  $m$  subsamples is good is given by

$$P = 1 - [1 - (1 - \varepsilon)^p]^m . \quad (12)$$

By requiring that  $P$  must be near 1, one can determine  $m$  for given values of  $p$  and  $\varepsilon$ . In our implementation, we assume  $\varepsilon = 40\%$  and require  $P = 0.99$ , thus  $m = 272$ . Note that the algorithm can be speeded up considerably by means of parallel computing, because the processing for each subsample can be done independently.

As noted in [48], the LMedS *efficiency* is poor in the presence of Gaussian noise. The efficiency of a method is defined as the ratio between the lowest achievable variance for the estimated parameters and the actual variance provided by the given method. To compensate for this deficiency, we further carry out a weighted least-squares procedure. The *robust standard deviation* estimate is given by

$$\hat{\sigma} = 1.4826[1 + 5/(n - p)]\sqrt{M_J} ,$$

where  $M_J$  is the minimal median. The reader is referred to [48, page 202] for the explanation of these magic numbers. Based on  $\hat{\sigma}$ , we can assign a weight for each correspondence:

$$w_i = \begin{cases} 1 & \text{if } r_i^2 \leq (2.5\hat{\sigma})^2 \\ 0 & \text{otherwise ,} \end{cases}$$

where

$$r_i^2 = d^2(\tilde{\mathbf{m}}_{2i}, \mathbf{F} \tilde{\mathbf{m}}_{1i}) + d^2(\tilde{\mathbf{m}}_{1i}, \mathbf{F}^T \tilde{\mathbf{m}}_{2i}) .$$

The correspondences having  $w_i = 0$  are outliers and should not be further taken into account. The fundamental matrix  $\mathbf{F}$  is finally estimated by solving the weighted least-squares problem:

$$\min \sum_i w_i r_i^2 .$$

We have thus robustly estimated the fundamental matrix because outliers have been detected and discarded by the LMedS method.

As said previously, computational efficiency of the LMedS method can be achieved by applying a Monte-Carlo type technique. However, the eight points of a subsample thus generated may be very close to each other. Such a situation should be avoided because the estimation of the epipolar geometry from such points is highly instable and the result

is useless. It is a waste of time to evaluate such a subsample. In order to achieve higher stability and efficiency, we develop a *regularly random selection method* based on bucketing techniques, which works as follows. We first calculate the **min** and **max** of the coordinates of the points in the first image. The region is then evenly divided into  $b \times b$  buckets (see Fig. 4). To each bucket is attached a set of points, and indirectly a set of matches, which fall in it. The buckets having no matches attached are excluded. To generate a subsample of 8 points, we first randomly select 8 mutually different buckets, and then randomly choose one match in each selected bucket.

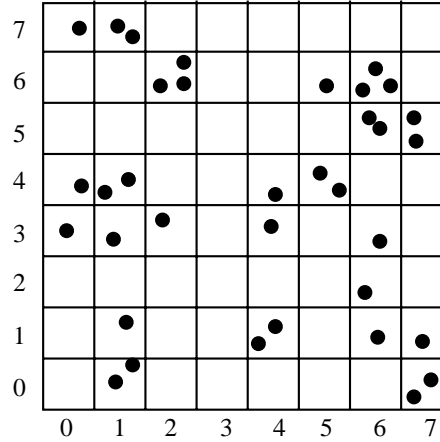


Fig. 4. Illustration of a bucketing technique

One question remains: How many subsamples are required? If we assume that bad matches are uniformly distributed in space, and if each bucket has the same number of matches and the random selection is uniform, the formula (12) still holds. However, the number of matches in one bucket may be quite different from that in another. As a result, a match belonging to a bucket having fewer matches has a higher probability to be selected. It is thus preferred that a bucket having many matches has a higher probability to be selected than a bucket having few matches, in order that each match has almost the same probability to be selected. This can be realized by the following procedure. If we have in total  $l$  buckets, we divide  $[0, 1]$  into  $l$  intervals such that the width of the  $i^{\text{th}}$  interval is equal to  $n_i / \sum_i n_i$ , where  $n_i$  is the number of matches attached to the  $i^{\text{th}}$  bucket (see Fig. 5). During the bucket selection procedure, a number, produced by a  $[0, 1]$  uniform random generator, falling in the  $i^{\text{th}}$  interval implies that the  $i^{\text{th}}$  bucket is selected.

In our implementation,  $b = 8$ .

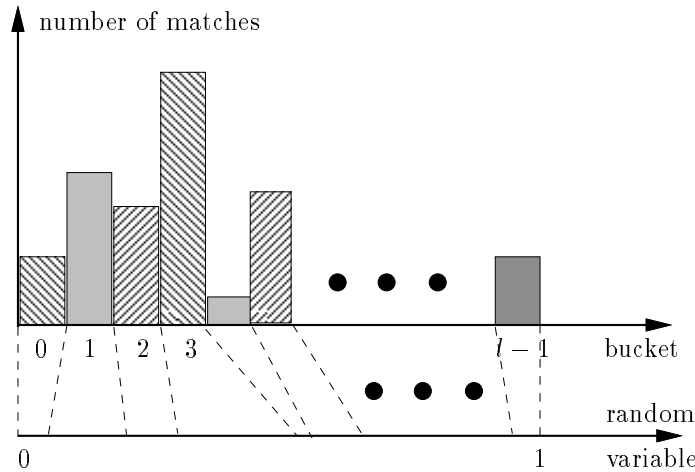


Fig. 5. Interval and bucket mapping

## 7 Stereo Matching

Once the fundamental matrix has been determined robustly, we use it to establish a new set of correspondences using a correlation based approach that takes into account the recovered epipolar geometry (i.e., epipolar constraint).

The matching approach that has been developed is a slightly modified version of the initial matching process (Sect. 4). For a feature point in the first image, and in order to find possible matching partners not too far from the epipolar line in the second image, we place a narrow band of width  $2\epsilon$  pixels centered on this epipolar line and find the points that lie within the band. The value of  $\epsilon$  is chosen to be  $3.8\bar{d}$  for a probability of 95%, where  $\bar{d}$  is the root of mean squares of distances between the points and their epipolar lines defined by the recovered fundamental matrix, i.e.,  $\bar{d} = \sqrt{\sum_i w_i r_i^2 / \sum_i w_i}$ . The same constraints as in Sect. 4 are then applied to select the most consistent matches, except that the constraint on the disparity (defined by the search window) is replaced by the epipolar constraint just described.

If needed, we can refine the estimation of the fundamental matrix using all correspondences established at this point. The number of correspondences found in this step is usually larger.

## 8 Experimental Results

The proposed algorithm has been tested on two dozen image pairs, and good results have been obtained. Different types of scenes have been used, such as indoor, rocks, road, and

textured dummy scenes. Due to space limitation, we provide in this paper the matching results of six image pairs, which are labeled **bust**, **road**, **valley**, **rotation**, **trunk** and **tracing**. The last image pair has been generated by a ray-tracing algorithm, and contains many repetitive patterns. All others are real images. The image resolution is  $512 \times 512$ , except for scene **road**, whose resolution is  $512 \times 470$ . All parameters used in the algorithm are the same for all image pairs with one exception, and are as were specified in the previous sections. The exception was done for image pair **rotation**. Because of its large disparity in  $y$ -direction, the size of correlation search window, which is set to  $257 \times 257$  by default, is not big enough, and we have set it to  $257 \times 301$ .

In order to show the performance of the relaxation procedure, we also provide the matching results given by the correlation technique. The correlation results are obtained as follows. We perform the correlation twice by reversing the roles of the two images (i.e., from left to right, and then from right to left) and consider as valid only those matches for which the reverse correlation has fallen on the initial point in the first image. More precisely, for a given point  $\mathbf{m}_1$  in the left image, let the match candidate with the highest correlation score be  $\mathbf{m}_2$  through a left-to-right correlation. Before validating the match, we perform a right-to-left correlation. If the match candidate with the highest correlation score for  $\mathbf{m}_2$  is again  $\mathbf{m}_1$ , then this match will be validated; otherwise, it will be rejected. The two images thus play a symmetric role. This validity test allows us to reduce greatly the probability of error.

**Table 1.** Summary of the matching results with the correlation, relaxation and robust methods: Numbers of total and bad matches

Scene name	Nbr of Pts (left - right)	Correlation (total/bad)	Relaxation (total/bad)	LMedS (detected)	Stereo (matches)	Nbr of iterations
<b>bust</b>	512 - 512	103/4	97/0	11	93	11
<b>road</b>	367 - 389	53/12	52/7	5	48	12
<b>valley</b>	395 - 512	235/14	248/4	15	241	16
<b>rotation</b>	288 - 255	89/31	102/11	15	88	12
<b>trunk</b>	377 - 355	117/25	127/20	22	118	15
<b>tracing</b>	383 - 352	143/ <i>lots</i>	248/19	31	226	20

The results are shown in figures 6 through 23, and are summarized in table 1. For each scene, three figures are provided, showing the matching results by correlation, relaxation and stereo. By stereo is meant that the epipolar geometry estimated by the robust method LMedS is used in matching, as described in Sect. 7. In each figure, two pictures (the left and right images) are shown. Points are indicated by a cross, and matched points are given the same number. The epipolar lines are drawn on the images to illustrate the difference between the epipolar geometry estimated from all matches found by relaxation and that

estimated by the LMedS. In table 1, both the total number of matches and the number of bad matches found by correlation and relaxation are provided, together with the number of outliers detected by the LMedS and the number of matches found by stereo. Here, we only count false matches as bad matches, and do not take into account those matches due to bad location. The LMedS actually detects all those bad matches except for scene **road**, and the matches due to bad locations. Sometimes, the LMedS also rejects a few good matches whose error measures go slightly beyond the threshold defined in Sect.6.3. The last column shows the number of iterations conducted during the relaxation process. The word *lots* in the last row means that the number of bad matches is very high (more than 50% and not checked carefully) when the correlation technique was used for scene **tracing**. Just for information, the first column gives the number of points of interest for each of the first and second images.

**Table 2.** Comparison of the normalized residuals before and after discarding outliers by LMedS (in pixels)

	<b>bust</b>	<b>road</b>	<b>valley</b>	<b>rotation</b>	<b>trunk</b>	<b>tracing</b>
before	0.6	5.1	3.8	9.2	13.0	8.5
after	0.3	0.8	0.7	0.5	1.2	0.4

In Table 2, the normalized residuals before and after discarding outliers by LMedS are given, which show the improvement achieved by incorporating an outlier detection module. A normalized residual is approximately equal to the average distance between a point and its epipolar line.

For scene **bust** (Figs. 6–8), the images were taken by two cameras with parallel optical axes placed almost horizontally. There were a few false matches when using the correlation technique, e.g., match 76 (on the right part of the images in Fig. 6). The matches found with the relaxation are all correct. The epipolar geometry computed from these matches is shown by the epipolar lines in Fig. 7. The average distance between a point and its epipolar line is 0.6 pixels. Consider that the precision of a point extracted by the corner detector described in Sect. 4.1 is in the order of one pixel, the epipolar geometry estimated is quite good. Two good matches found by correlation are missed by relaxation: matches 4 and 15 in the top part of images in Fig. 6. This is because these matches are isolated and too far away from other matches to gain any support. Recall that the radius of the neighborhood disc  $R$  is set to the eighth of the image width. If we increase the value of  $R$ , we can recover these two matches. Although all matches are correct, LMedS still detects 11 matches as outliers, and the average distance between a point and its epipolar line is now reduced to 0.3 pixels. Comparing the epipolar geometry illustrated in Fig. 8 with that in Fig. 7, one can hardly find any difference.

For scene **road** (Figs.9–11), the two images were taken by a single camera mounted on a moving vehicle (this is thus a motion sequence). The vehicle moves forward on the right lane, and the epipolar lines are thus expected to intersect to each other at a point near the

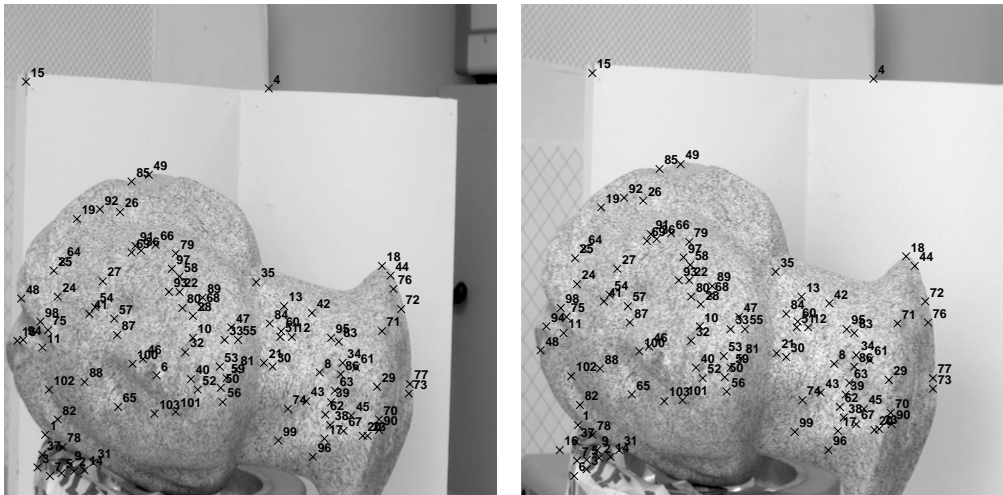


Fig. 6. Scene bust: Matching result with the correlation technique

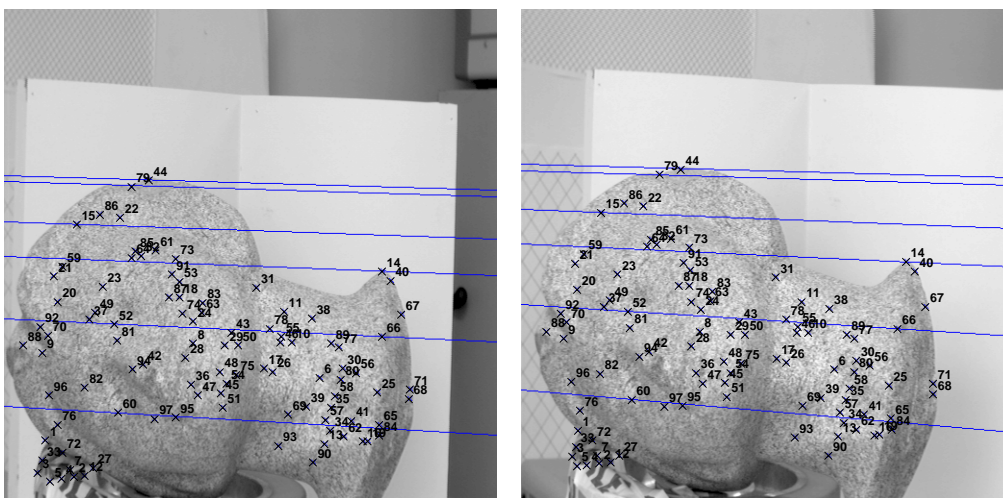


Fig. 7. Scene bust: Matching result with the relaxation technique and the epipolar geometry recovered using all matched points

center of the image. Figure 9 shows the matched points recovered by using the correlation technique. One can notice that some points have not been correctly matched: matches 5, 21 and 23, to name a few. After carrying out the relaxation procedure, several false matches have been corrected, but a few still persist, e.g., match 22 in Fig. 10. The epipolar geometry

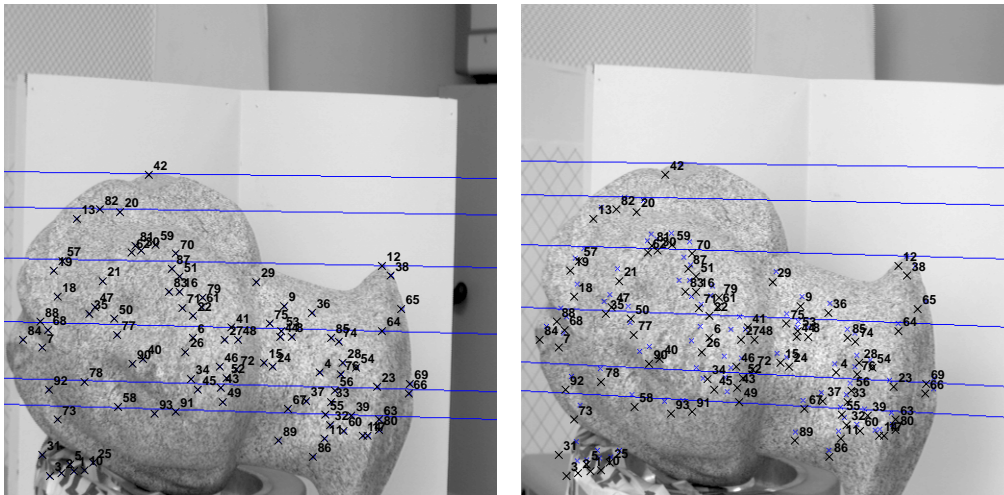


Fig. 8. Scene bust: The epipolar geometry recovered after discarding outliers and the matched points found using the epipolar constraint

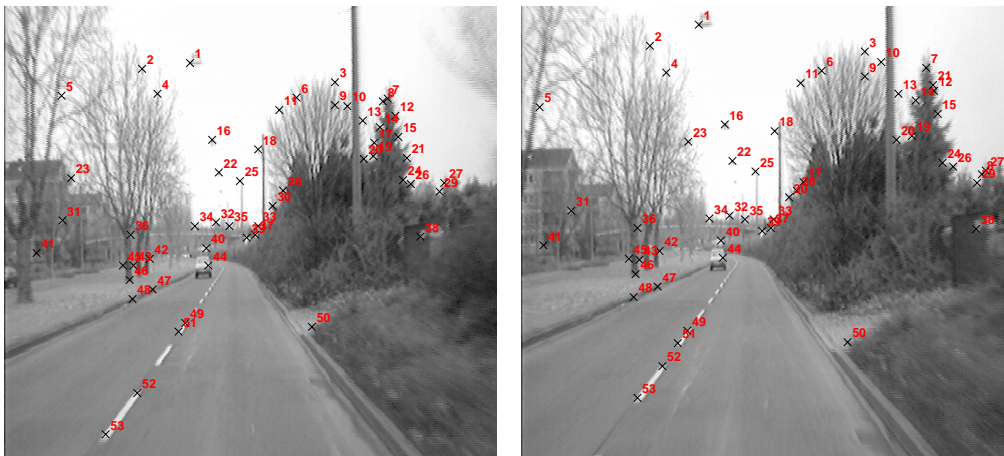


Fig. 9. Scene road: Matching result with the correlation technique

estimated, as shown by the epipolar lines in Fig. 10, is not correct, and the average distance between a point and its epipolar line is 5.1 pixels, which is quite large. The LMedS has detected and rejected 5 outliers (3 false matches and 2 not very well located points). This significantly changes the epipolar geometry, in particular, the positions of the epipoles, as

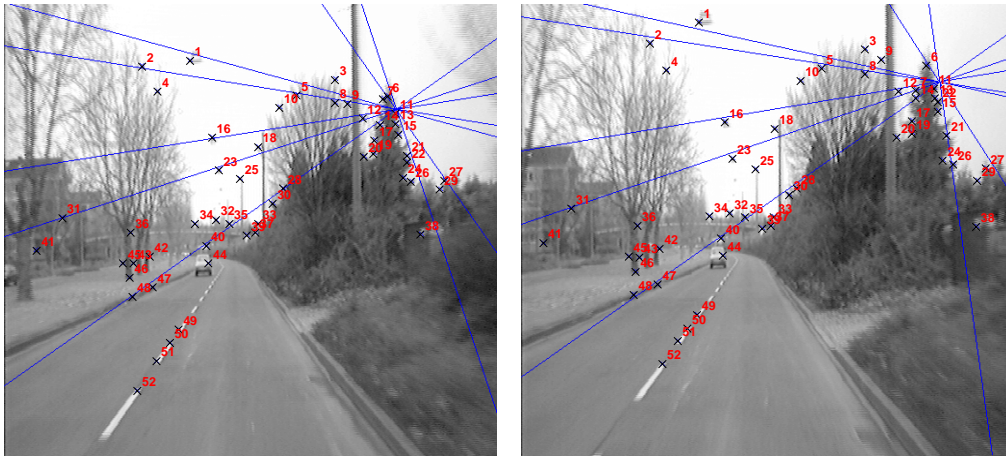


Fig. 10. Scene road: Matching result with the relaxation technique and the epipolar geometry recovered using all matched points

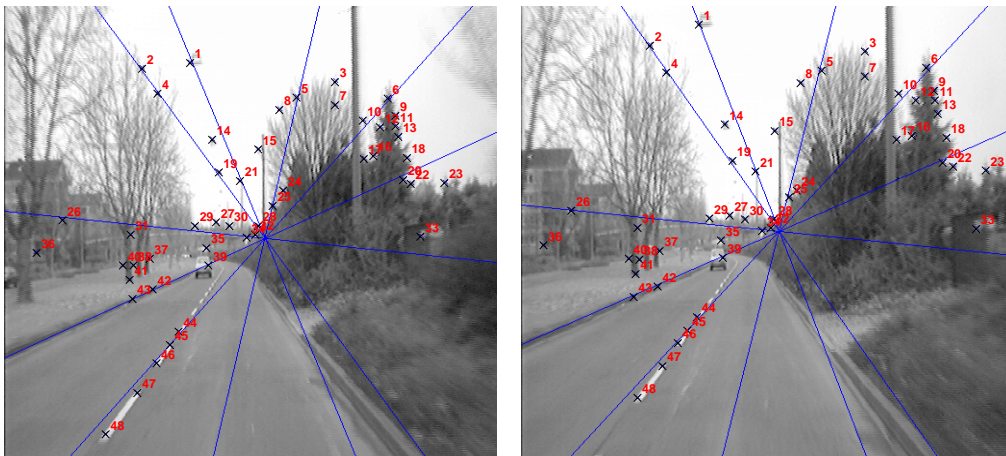


Fig. 11. Scene road: The epipolar geometry recovered after discarding outliers and the matched points found using the epipolar constraint

shown in Fig. 11. The average distance is now 0.8 pixels. The attentive reader may have noticed that the number of outliers detected, 5, is less than the number of false matches, 7 (see Table 1). In fact, there are four matches (49, 50, 51 and 52 in Fig. 10) on the lane marker

which are not correct. However, they have not been detected by the LMedS because they almost lie on the same epipolar line (see Fig. 11). As the criterion used in outlier detection is the epipolar constraint, false matches lying on the epipolar line cannot be detected by our LMedS method.

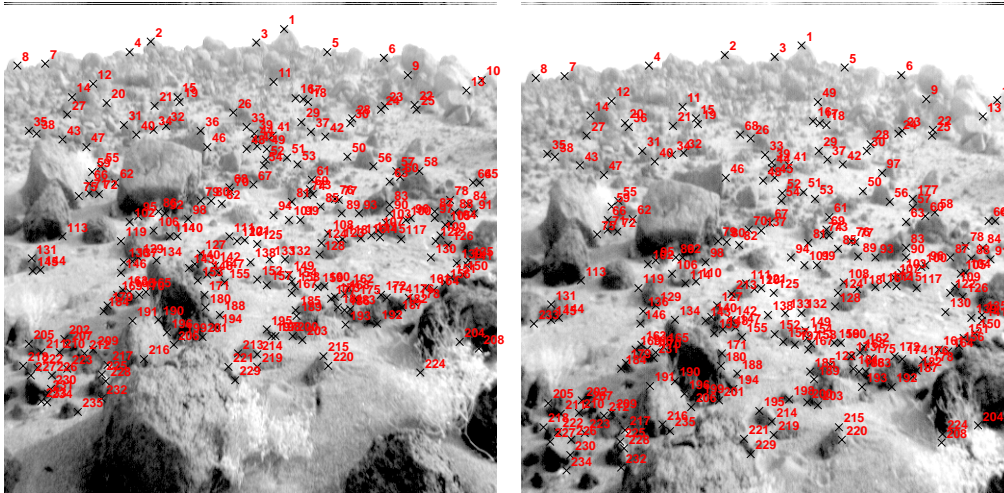


Fig. 12. Scene valley: Matching result with the correlation technique

For scene **valley** (Figs.12–14), the two images were taken by two cameras placed one above the other. The epipolar lines are thus expected to be almost parallel and oriented vertically. The scene is composed of rocks with different sizes. As the scene is rather textured, the correlation technique works reasonably well: 235 matches have been found, 14 of which are false (see Fig. 12). After the relaxation process, even more matches (248) have been recovered, and only four of them are false. The false matches are those labeled 184, 54, 49 and 214 in Fig. 13. Although there are only four false matches, the epipolar geometry estimated is completely wrong, as shown by the epipolar lines in Fig. 13, and the average distance between a point and its epipolar line is 3.8 pixels, which is large. The LMedS has detected all these false matches plus several not very well located ones. This completely changes the epipolar geometry, as shown in Fig. 14. The average distance is now 0.7 pixels.

For scene **rotation** (Figs.15–17), the two images were taken by the same camera, but there is a rotation around the optical center and a tilt translation between the two positions. In spite of the image distortion due to the rotation, the correlation works reasonably except for the points on the grid against the wall, where the repetitive patterns make matching by correlation extremely difficult (see Fig. 15): among 89 matches recovered, 31 are false. Because of the use of contextual (neighboring) information, the relaxation technique has produced a much better matching result (see Fig. 16). Among 102 matches recovered, only 11 are false, and almost all matches on the grid are correct. The LMedS has detected all

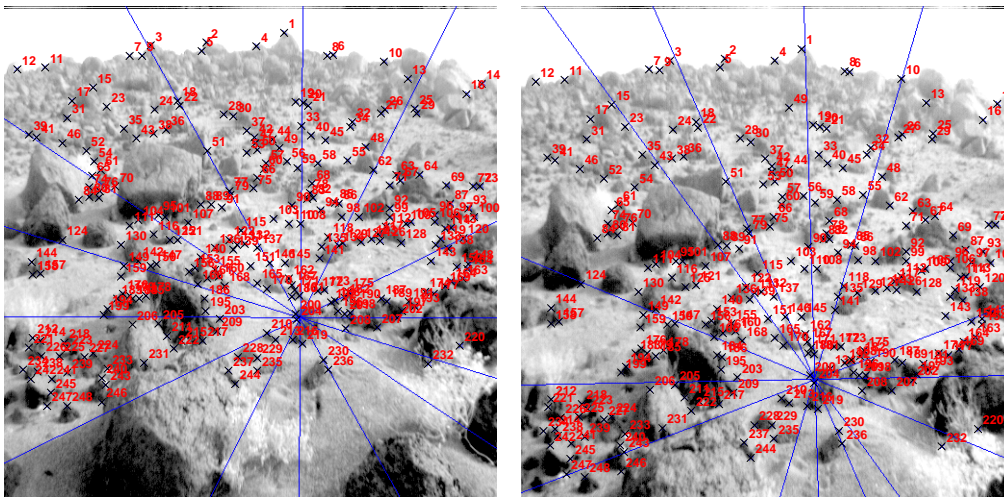


Fig. 13. Scene valley: Matching result with the relaxation technique and the epipolar geometry recovered using all matched points

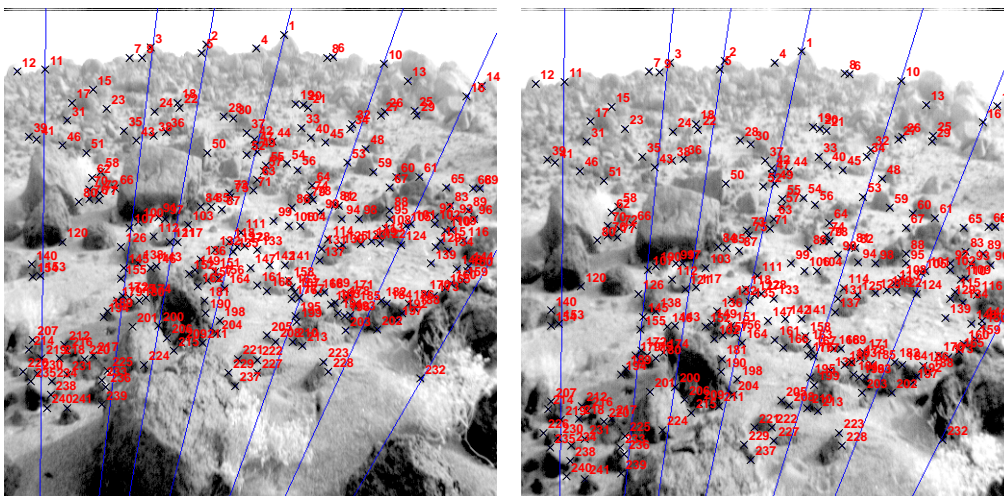


Fig. 14. Scene valley: The epipolar geometry recovered after discarding outliers and the matched points found using the epipolar constraint

the false matches, and the epipolar geometry estimated is illustrated by lines in Fig. 17. The average distance between a point and its epipolar line is reduced from 9.2 pixels to 0.5.

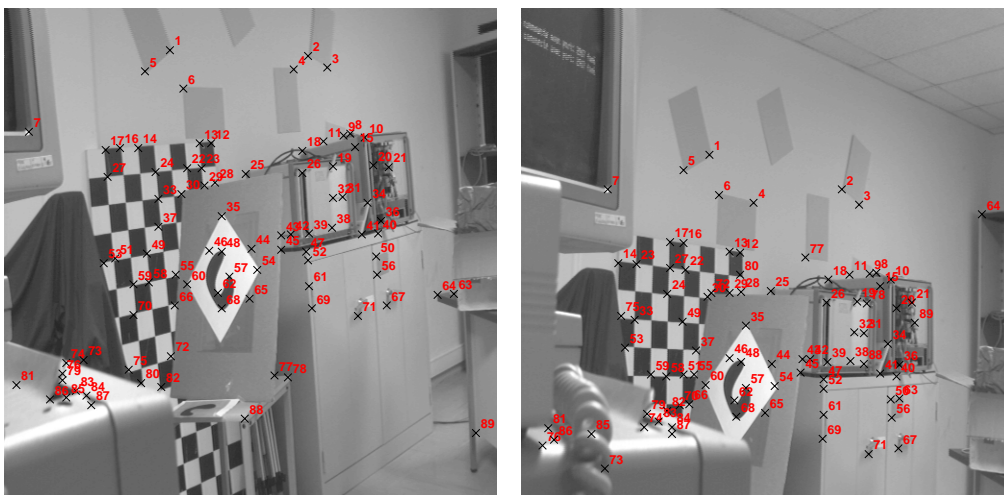


Fig. 15. Scene rotation: Matching result with the correlation technique

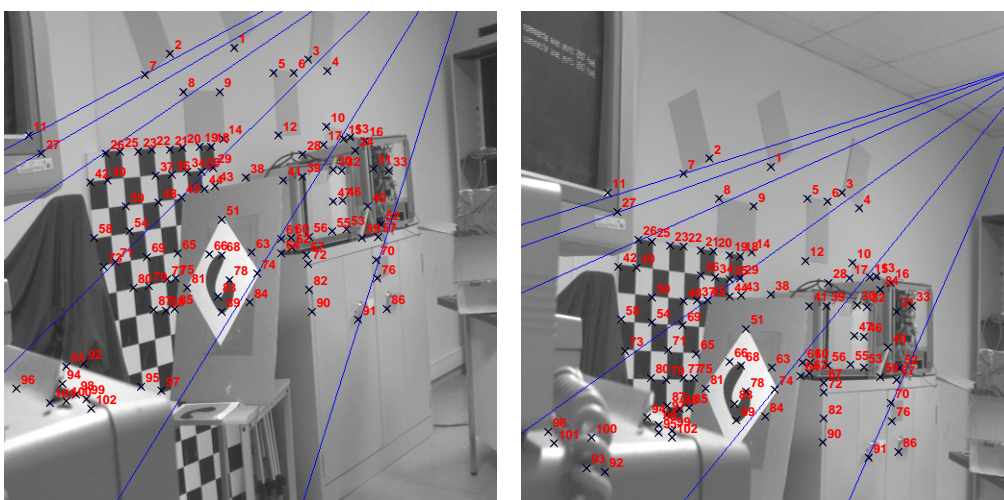


Fig. 16. Scene rotation: Matching result with the relaxation technique and the epipolar geometry recovered using all matched points

For scene **trunk** (Figs.18–20), the two images were taken by two cameras placed side by side. The two cameras have quite different focal lengths, as can be noticed by the change of the trunks' size. Again, despite the scale difference, our method works well. One can also notice the drastic change in the epipolar geometry estimated before (Fig. 19) and after

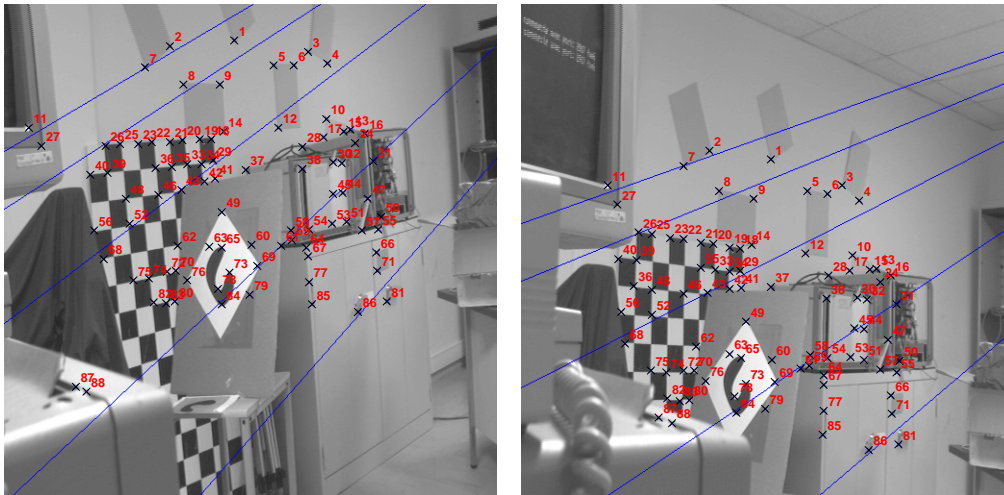


Fig. 17. Scene rotation: The epipolar geometry recovered after discarding outliers and the matched points found using the epipolar constraint



Fig. 18. Scene trunk: Matching result with the correlation technique

(Fig. 20) applying the LMedS technique for outlier detection. The average distance between a point and its epipolar line is reduced from 13 pixels to 1.2.

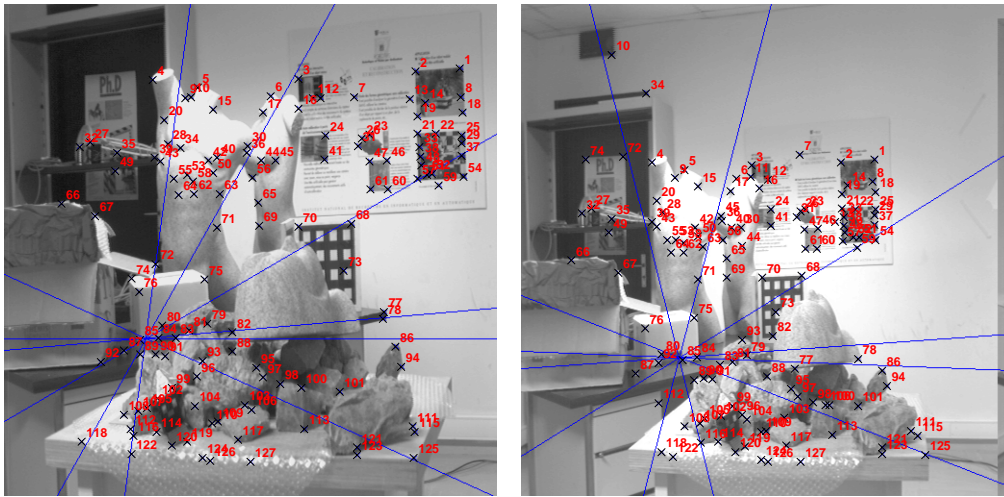


Fig. 19. Scene trunk: Matching result with the relaxation technique and the epipolar geometry recovered using all matched points

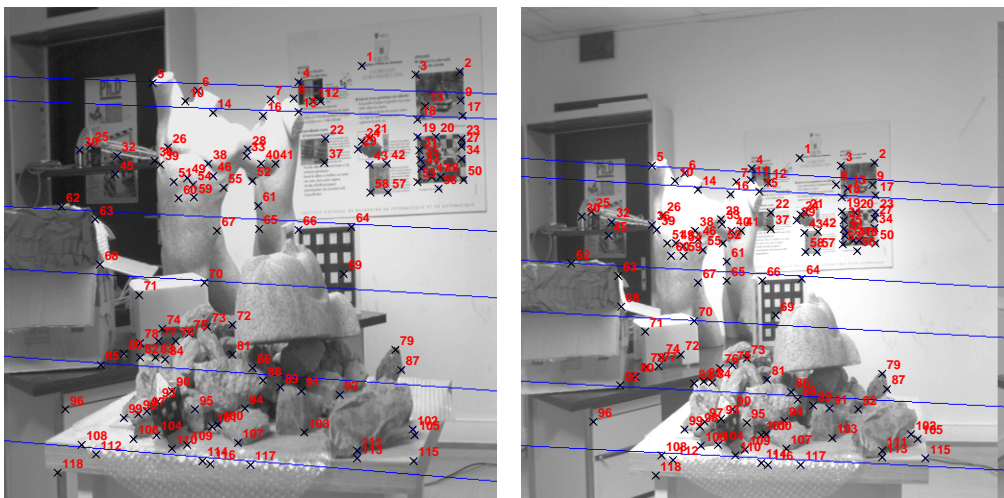


Fig. 20. Scene trunk: The epipolar geometry recovered after discarding outliers and the matched points found using the epipolar constraint

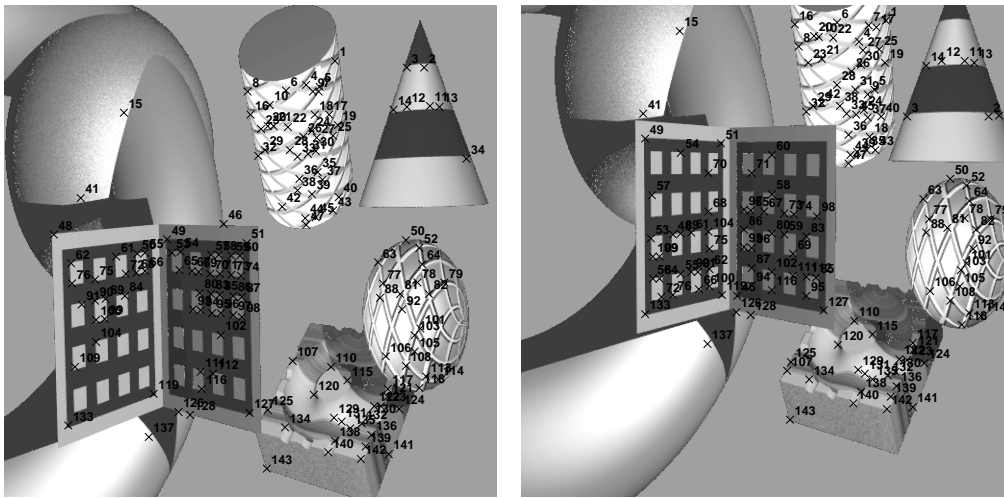


Fig. 21. Scene tracing: Matching result with the correlation technique

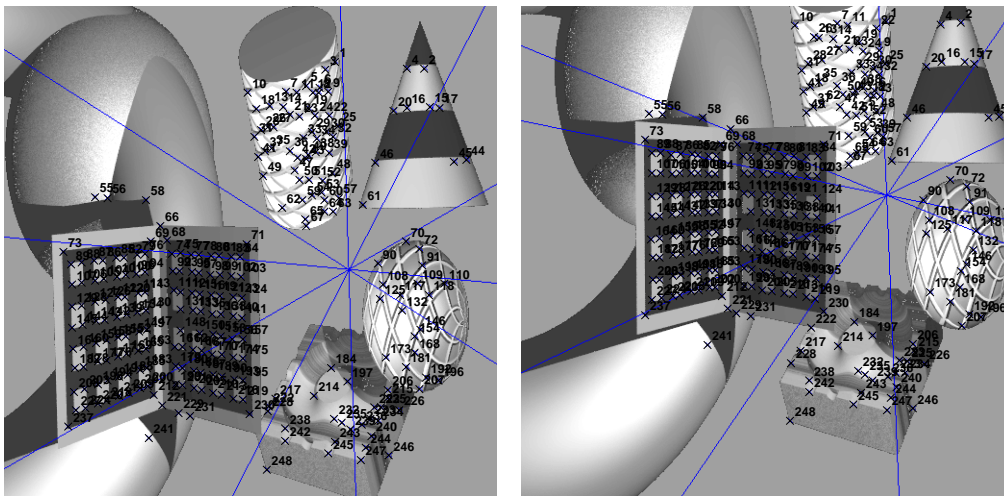


Fig. 22. Scene tracing: Matching result with the relaxation technique and the epipolar geometry recovered using all matched points

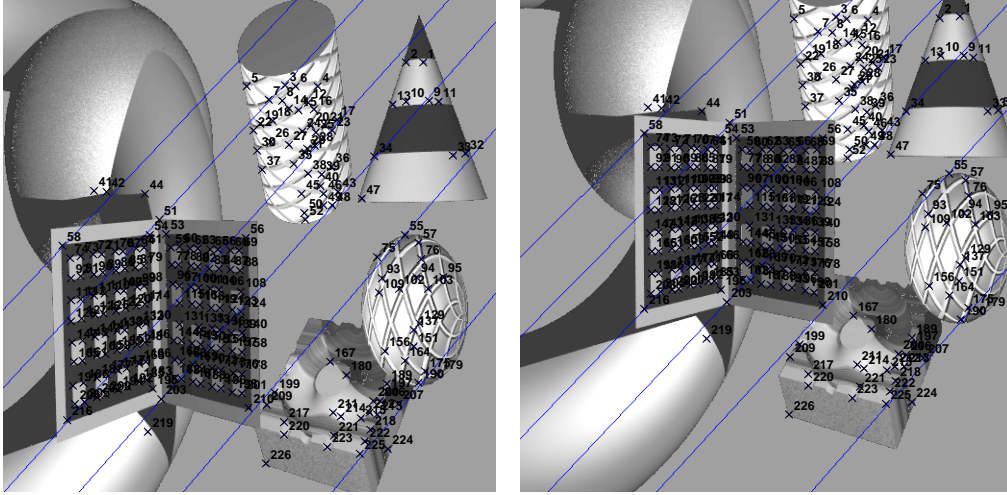


Fig. 23. Scene tracing: The epipolar geometry recovered after discarding outliers and the matched points found using the epipolar constraint

Finally, the two images in scene **tracing** (Figs.21–23) were generated by a ray tracing technique simulating two cameras placed diagonally. The numerous repetitive patterns make the matching by correlation almost impossible. Indeed, among 143 matches found, more than a half are false (Fig.21). This implies that if we apply the LMedS at this stage we cannot obtain any useful result. Using the relaxation technique, we have obtained a very good matching result: 248 matches have been recovered, and only 19 are false (Fig.22). These false matches have been all detected by the LMedS, and the epipolar geometry has been correctly estimated, as shown in Fig.23. The average distance between a point and its epipolar line is reduced from 8.5 pixels in Fig.22 to 0.4 pixels in Fig.23. The fundamental matrix used for generating the two images is:

$$\begin{bmatrix} 6.440951e-07 & 5.203664e-06 & 1.658593e-02 \\ -4.065228e-06 & 7.716572e-07 & 1.798488e-02 \\ -1.821295e-02 & -1.834903e-02 & 1 \end{bmatrix}$$

and the estimated one is:

$$\begin{bmatrix} 6.455367e-07 & 5.146858e-06 & 1.622137e-02 \\ -4.012881e-06 & 7.702527e-07 & 1.775179e-02 \\ -1.785370e-02 & -1.811788e-02 & 1 \end{bmatrix}$$

For comparison, we have normalized the last element to 1. The difference between them is very small.

In Table 3, we summarize the CPU time in seconds spent in each step on a Spar 10 Workstation. The time shown is merely indicative, as we have not tried to optimize our

**Table 3.** Computation time in each step: CPU time in seconds on a Sparc 10 Workstation

Scene	Correlation	Relaxation	LMedS	Stereo
<b>bust</b>	16.9	5.9	2.2	1.8
<b>road</b>	8.4	1.9	1.5	2.0
<b>valley</b>	8.6	9.5	3.3	1.6
<b>rotation</b>	2.8	2.1	2.0	0.6
<b>trunk</b>	6.3	4.9	2.1	2.0
<b>tracing</b>	6.1	76	3.2	1.1

codes. The time for correlation depends on the scene complexity, and essentially the number of points. The time for relaxation depends on the degree of matching ambiguity. If there are not many matching candidates, like in scene **road**, the time is very short. In scene **tracing**, however, the time spent in relaxation is extremely high (76 seconds!) because each point may have as many as 40 matching candidates. The time for LMedS is almost constant, around 2 seconds. The time for stereo is around 1.6 seconds. Thus, in general, the most time consuming step is the correlation.

## 9 Conclusion

We have proposed in this paper a robust approach to image matching by exploiting the only geometric constraint, namely, the epipolar constraint. The presence of the epipolar geometry between two images is now well known, and can be described by the fundamental matrix. The idea is to use some heuristic techniques (correlation methods in our particular implementation) to find an initial set of matches, and then use a very robust technique—the Least Median of Squares (LMedS)—to discard outliers in this set. The LMedS aims at finding the fundamental matrix, by searching in the parameter space, which minimizes the median of the squared errors. An error is quantified by the distance of a point to its corresponding epipolar line. This method has been tested with a large number of real images (indoor scenes, outdoor scenes, dummy mannequins, etc.). From the experiments we have carried out, our approach allows about 40% of false matches in the initial set of matches. The fundamental matrix can finally be accurately estimated from the good points.

There still exist a number of ways to improve our algorithm:

**Accuracy** The precision of the final estimation of the fundamental matrix depends tightly on those of the matched points. To have a better estimation of the fundamental matrix, we should increase the accuracy of matched points. One possibility is to use subpixel-precision corner detector whenever possible. For example, if we are working in an indoor environment, we may use corner detectors such as [11, 46, 8]. Another possibility is to apply subpixel-precision correlation techniques. The idea is to compute the correlation

score for each point in the neighborhood of the match, and fit a parametric surface, e.g., a paraboloid, to the correlation scores, and eventually compute the position with the largest correlation score.

**Stability** The stability of our algorithm is directly related to that of finding the fundamental matrix, which is studied in [33]. One of the most stringent situations is that all points are located close to a critical surface, for example, a plane. If the points are almost on a plane, it is better to describe their relation between two views by a homography instead of a fundamental matrix. This will not change considerably the structure of our algorithm. The question is when to switch from using a fundamental matrix to using a homography, and vice versa.

**Ambiguity** Using the epipolar constraint alone does not allow to find unambiguous matches between two views. If a false match is occasionally aligned with the epipolar line, it will not be detected by our algorithm because only the epipolar constraint is used for outlier rejection. This of course does not disturb the estimation of the fundamental matrix. A good stereo matching algorithm, such as [44, 34], should be used to exploit other constraints like a disparity gradient limit.

## Acknowledgment

The authors thank Thierry Blaszkza for the corner detection code, Cyril Zeller for the correlation code and various discussions, and Charles Rothwell for checking the English.

## References

- [1] J.K. Aggarwal and N. Nandhakumar. On the computation of motion from sequences of images — a review. *Proc. IEEE*, 76(8):917–935, August 1988.
- [2] H. Asada and M. Brady. The curvature primal sketch. *IEEE Transactions on Pattern Analysis and Machine Intelligence*, 8:2–14, 1986.
- [3] S. Ayer, P. Schroeter, and J. Bigun. Segmentation of moving objects by robust motion parameter estimation over multiple frames. In J.-O. Eklundh, editor, *Proc. Third European Conf. Comput. Vision*, pages 316–327, Vol.II, Stockholm, Sweden, May 1994.
- [4] D. H. Ballard and C. M. Brown. *Computer Vision*. Prentice-Hall, Englewood Cliffs, NJ, 1982.
- [5] S.T. Barnard and W.B. Thompson. Disparity analysis of images. *IEEE Trans. PAMI*, 2(4):333–340, July 1980.
- [6] J.K. Cheng and T.S. Huang. Image registration by matching relational structures. *Pattern Recog.*, 17(1):149–159, 1984.

- 
- [7] C.-H. Chou and Y.-C. Chen. Moment-preserving pattern matching. *Pattern Recog.*, 23(5):461–474, 1990.
  - [8] R. Deriche and T. Blaszk. Recovering and characterizing image features using an efficient model based approach. In *Proc. International Conference on Computer Vision and Pattern Recognition*, New-York, June 14-17 1993.
  - [9] R. Deriche and O. Faugeras. Tracking line segments. In O. Faugeras, editor, *Proc. First European Conf. Comput. Vision*, pages 259–268, Antibes, France, April 1990. Springer, Berlin, Heidelberg.
  - [10] R. Deriche and O.D. Faugeras. 2D-curves matching using high curvatures points : Applications to stereovision. In *Proc. 10th Int'l Conf. Pattern Recog.*, pages 240–242, Vol.1, Atlantic City, June 16-21 1990.
  - [11] R. Deriche and G. Giraudon. A computational approach for corner and vertex detection. *The International Journal of Computer Vision*, 10(2):101–124, 1993.
  - [12] R. Deriche, Z. Zhang, Q.-T Luong, and O. Faugeras. Robust recovery of the epipolar geometry for an uncalibrated stereo rig. In *Proc. Third European Conf. Comput. Vision*, pages 567–576, Vol.I, May 1994.
  - [13] O.D. Faugeras, F. Lustman, and G. Toscani. Motion and structure from motion from point and line matches. In *Proc. First Int'l Conf. Comput. Vision*, pages 25–34, London, UK, 1987.
  - [14] P. Fua. A parallel stereo algorithm that produces dense depth maps and preserves image features. *Machine Vision and Applications*, 6(1), Winter 1993.
  - [15] A. Goshtasby, S. H. Gage, and J. F. Bartholic. A two-stage cross correlation approach to template matching. *IEEE Trans. PAMI*, 6(3):374–378, May 1984.
  - [16] M.J. Hannah. A system for digital stereo image matching. *Photogrammetric Engineering and Remote Sensing*, 55(12):1765–1770, December 1989.
  - [17] R.M. Haralick. Computer vision theory: The lack thereof. *Comput. Vision, Graphics Image Process.*, 36:372–386, 1986.
  - [18] R.M. Haralick et al. Pose estimation from corresponding point data. *IEEE Trans. SMC*, 19(6):1426–1446, November 1989.
  - [19] C. Harris and M. Stephens. A combined corner and edge detector. In *Proceedings Alvey Conference*, pages 189–192, 1988.
  - [20] C.G. Harris. Determination of ego-motion from matched points. In *Proceedings Alvey Conference*, 1987.

- 
- [21] R. Horaud and F. Veillon. Finding geometric and relational structures in an image. In *Proc. First European Conference On Computer Vision*, pages 374–384, 1990.
- [22] R. Horaud and Th. Skordas. Stereo correspondence through feature grouping and maximal cliques. *IEEE Trans. PAMI*, 11(11):1168–1180, 1989.
- [23] T.S. Huang and O.D. Faugeras. Some properties of the E matrix in two-view motion estimation. *IEEE Trans. PAMI*, 11(12):1310–1312, December 1989.
- [24] T.S. Huang and A.N. Netravali. Motion and structure from feature correspondences: A review. *Proc. IEEE*, 82(2):252–268, February 1994.
- [25] P.J. Huber. *Robust Statistics*. John Wiley & Sons, New York, 1981.
- [26] R. Kumar and A.R. Hanson. Analysis of different robust methods for pose refinement. In *Proc. Int'l Workshop Robust Comput. Vision*, pages 167–182, Seattle, WA, October 1990.
- [27] C.-H. Lee. Time-varying images: The effect of finite resolution on uniqueness. *CVGIP: Image Understanding*, 54(3):325–332, 1991.
- [28] S.Z. Li. Inexact matching of 3D surfaces. Technical Report VSSP-TR-3/90, Vision Speech & Signal Processing, Dept. Electronic and Electrical Engineering, University of Surrey, UK, February 1990.
- [29] H.C. Longuet-Higgins. A computer algorithm for reconstructing a scene from two projections. *Nature*, 293:133–135, 1981.
- [30] H.C. Longuet-Higgins. The reconstruction of a scene from two projections - configurations that defeat the 8-point algorithm. In *Proc. First Conf. Artif. Intell. Applications*, pages 395–397, Denver, Colorado, 1984.
- [31] Q.-T. Luong. *Matrice fondamentale et calibration visuelle sur l'environnement: Vers une plus grande autonomie des systèmes robotiques*. Dissertation, University of Paris XI, Orsay, Paris, France, December 1992.
- [32] Q.-T. Luong, R. Deriche, O. Faugeras, and T. Papadopoulos. On determining the fundamental matrix: Analysis of different methods and experimental results. Rapport de Recherche 1894, INRIA Sophia-Antipolis, France, 1993.
- [33] Q.-T. Luong and O. Faugeras. A stability analysis of the fundamental matrix. In J.-O. Eklundh, editor, *Proc. Third European Conf. Comput. Vision*, pages 577–588, Stockholm, Sweden, May 1994. Springer-Verlag Berlin.
- [34] R. Ma, M. Thonnat, and M. Berthod. An adjustment-free stereo matching algorithm. In J. Illingworth, editor, *Proc. British Machine Vision Conf.*, pages 609–618, University of Surrey, Guildford, UK, September 1993. BMVA Press.

- 
- [35] H. Maître and Yifeng Wu. Improving dynamic programming to solve image registration. *Pattern Recog.*, 20(4):443–462, 1987.
- [36] S.J. Maybank and O.D. Faugeras. A theory of self-calibration of a moving camera. *Int'l J. Comput. Vision*, 8(2):123–152, August 1992.
- [37] G. Medioni and Y. Yasumoto. Corner detection and curve representation using cubic b-spline. In *Proc. International Conference on Robotics and Automation*, pages 764–769, 1986.
- [38] P. Meer, D. Mintz, A. Rosenfeld, and D.Y. Kim. Robust regression methods for computer vision: A review. *Int'l J. Comput. Vision*, 6(1):59–70, 1991.
- [39] H. Nagel. Image sequences - ten (octal) years- from phenomenology towards a theoretical foundation. In *Proc. 8th Int'l Conf. Pattern Recog.*, pages 1174–1185, Paris, France, October 1986. IEEE.
- [40] E. Nishimura, G. Xu, and S. Tsuji. Motion segmentation and correspondence using epipolar constraint. In *Proc. 1st Asian Conf. Computer Vision*, pages 199–204, Osaka, Japan, 1993.
- [41] J.A. Noble. Finding corners. *Image and Vision Computing*, 6:121–128, May 1988.
- [42] J.-M. Odobez and P. Bouthemy. Robust multiresolution estimation of parametric motion models applied to complex scenes. Publication interne 788, IRISA-INRIA Rennes, France, January 1994.
- [43] S.I. Olsen. Epipolar line estimation. In *Proc. Second European Conf. Comput. Vision*, pages 307–311, Santa Margherita Ligure, Italy, May 1992.
- [44] S.B. Pollard, J.E.W. Mayhew, and J.P. Frisby. PMF: A stereo correspondence algorithm using a disparity gradient limit. *Perception*, 14:449–470, 1985.
- [45] B. Radig. Image sequence analysis using relational structures. *Pattern Recog.*, 17(1):161–167, 1984.
- [46] K. Rohr. Modelling and identification of characteristic intensity variations. *Image and Vision Computing*, 10(2):66–76, 1992.
- [47] A. Rosenfeld, R.A. Hummel, and S.W. Zucker. Scene labeling by relaxation operations. *IEEE Trans. SMC*, 6(4):420–433, 1976.
- [48] P.J. Rousseeuw and A.M. Leroy. *Robust Regression and Outlier Detection*. John Wiley & Sons, New York, 1987.
- [49] L. Shapiro and M. Brady. Rejecting outliers and estimating errors in an orthogonal regression framework. Tech.Report OUEL 1974/93, Dept. Engineering Science, University of Oxford, February 1993.

- 
- [50] L.G. Shapiro and R.M. Haralick. Structural description and inexact matching. *IEEE Trans. PAMI*, 3:504–519, September 1981.
- [51] W.B. Thompson, P. Lechleider, and E.R. Stuck. Detecting moving objects using the rigidity constraint. *IEEE Trans. PAMI*, 15(2):162–166, February 1993.
- [52] P.H.S. Torr and D.W. Murray. Outlier detection and motion segmentation. In S, editor, *Sensor Fusion VI, SPIE Vol.2059*, pages 432–443, Boston, 1993.
- [53] R.Y. Tsai and T.S. Huang. Uniqueness and estimation of three-dimensional motion parameters of rigid objects with curved surface. *IEEE Trans. PAMI*, 6(1):13–26, January 1984.
- [54] S. Ullman. *The Interpretation of Visual Motion*. MIT Press, Cambridge, MA, 1979.
- [55] J. Weng, N. Ahuja, and T.S. Huang. Matching two perspective views. *IEEE Trans. PAMI*, 14(8):806–825, August 1992.
- [56] J. Weng, T.S. Huang, and N. Ahuja. Motion and structure from two perspective views: Algorithms, error analysis and error estimation. *IEEE Trans. PAMI*, 11(5):451–476, May 1989.
- [57] G. Xu, E. Nishimura, and S. Tsuji. Image correspondence and segmentation by epipolar lines: Theory, algorithm and applications. Technical report, Dept. of Systems Engineering, Osaka University, Japan, July 1993.
- [58] Z. Zhang. Token tracking in a cluttered scene. *Int'l J. of Image and Vision Computing*, 12(2):110–120, March 1994. Also Research Report No.2072, INRIA Sophia-Antipolis, 1993.
- [59] Z. Zhang and O.D. Faugeras. Estimation of displacements from two 3D frames obtained from stereo. *IEEE Trans. PAMI*, 14(12):1141–1156, December 1992.
- [60] X. Zhuang, T. Wang, and P. Zhang. A highly robust estimator through partially likelihood function modeling and its application in computer vision. *IEEE Trans. PAMI*, 14(1):19–34, January 1992.
- [61] S.W. Zucker, Y.G. Leclerc, and J.L. Mohammed. Continuous relaxation and local maxima selection: Conditions for equivalence. *IEEE Trans. PAMI*, 3:117–127, March 1981.



---

Unité de recherche INRIA Lorraine, Technopôle de Nancy-Brabois, Campus scientifique,  
615 rue du Jardin Botanique, BP 101, 54600 VILLERS LÈS NANCY  
Unité de recherche INRIA Rennes, Irisa, Campus universitaire de Beaulieu, 35042 RENNES Cedex  
Unité de recherche INRIA Rhône-Alpes, 46 avenue Félix Viallet, 38031 GRENOBLE Cedex 1  
Unité de recherche INRIA Rocquencourt, Domaine de Voluceau, Rocquencourt, BP 105, 78153 LE CHESNAY Cedex  
Unité de recherche INRIA Sophia-Antipolis, 2004 route des Lucioles, BP 93, 06902 SOPHIA-ANTIPOLIS Cedex

---

Éditeur  
INRIA, Domaine de Voluceau, Rocquencourt, BP 105, 78153 LE CHESNAY Cedex (France)  
ISSN 0249-6399